



HAL
open science

Impact of sediment provenance and depositional setting on chlorite content in Cretaceous turbiditic sandstones, Norway

Fares Azzam, Thomas Blaise, Patricia Patrier, Daniel Beaufort, Jocelyn Barbarand, Ahmed Abd Elmola, Benjamin Brigaud, Eric Portier, Sylvain Clerc

► To cite this version:

Fares Azzam, Thomas Blaise, Patricia Patrier, Daniel Beaufort, Jocelyn Barbarand, et al.. Impact of sediment provenance and depositional setting on chlorite content in Cretaceous turbiditic sandstones, Norway. *Basin Research*, 2024, 36 (3), pp.e12867. 10.1111/bre.12867. hal-04632597

HAL Id: hal-04632597

<https://cnrs.hal.science/hal-04632597>

Submitted on 2 Jul 2024




HAL is a multi-disciplinary open access archive for the deposit and dissemination of scientific research documents, whether they are published or not. The documents may come from teaching and research institutions in France or abroad, or from public or private research centers.

L'archive ouverte pluridisciplinaire **HAL**, est destinée au dépôt et à la diffusion de documents scientifiques de niveau recherche, publiés ou non, émanant des établissements d'enseignement et de recherche français ou étrangers, des laboratoires publics ou privés.



Distributed under a Creative Commons Attribution 4.0 International License

Impact of sediment provenance and depositional setting on chlorite content in Cretaceous turbiditic sandstones, Norway

Fares Azzam¹  | Thomas Blaise¹  | Patricia Patrier² | Daniel Beaufort² | Jocelyn Barbarand¹ | Ahmed Abd Elmola²  | Benjamin Brigaud¹ | Eric Portier³ | Sylvain Clerc⁴

¹Department of Geosciences, Université Paris-Saclay, CNRS, GEOPS, Orsay, France

²Department of Geosciences, Université de Poitiers, IC2MP—CNRS, Poitiers, France

³45-8 Energy, Metz, France

⁴Neptune Energy Norge AS, Sandnes, Norway

Correspondence

Fares Azzam and Thomas Blaise, Université Paris-Saclay, CNRS, GEOPS, Orsay 91405, France.
Email: fares.199@live.com and thomas.blaise@universite-paris-saclay.fr

Funding information

Neptune Energy Norge

Abstract

Chlorite minerals, mainly in the form of clay coats, play a critical role in determining the reservoir quality of siliciclastic rocks. They can positively influence reservoir quality by preserving porosity during deep burial, but they can also play a negative role by reducing permeability through pore filling. The main aim of this research is to determine the optimal conditions for chlorite growth in sedimentary basins. This study investigates the Lower Cretaceous turbidite sandstone of the Agat Formation in the North Sea. We used a source-to-sink approach to investigate the impact of sediment source composition, chemical weathering and depositional environment on chlorite formation. Understanding the interplay between these processes can help refine exploration and exploitation strategies, optimise hydrocarbon recovery, and reduce exploration risks. Representative samples from two hydrocarbon fields (the Duva and Agat fields) were investigated using petrography, geochemistry, heavy mineral identification and quantification, and U–Pb geochronology of detrital zircons. Our results show a strong heterogeneity in the sediment provenance between the two turbidite systems. In the Duva field, the sandstone is derived from a mixture of mafic and felsic sources, producing Fe-rich sediments. Intense chemical weathering generates fine fraction materials rich in kaolinite, vermiculite, and hydroxy-interlayered clays, which are transported into shallow marine settings. Subsequent interaction with seawater results in the formation of glauconitic materials, Fe-illite, and phosphatic concretions. These Fe-rich materials are remobilised into deep marine settings, providing precursors for the development of authigenic Fe-clays such as berthierine and chlorite. Conversely, in the Agat field, the sandstone is predominantly sourced from felsic rocks that underwent low chemical weathering, producing sediment rich in quartz and feldspar with a low amount of clays. With few Fe-rich materials transported into the basin, the development of chlorite in the Agat field was less

This is an open access article under the terms of the [Creative Commons Attribution](https://creativecommons.org/licenses/by/4.0/) License, which permits use, distribution and reproduction in any medium, provided the original work is properly cited.

© 2024 The Authors. *Basin Research* published by International Association of Sedimentologists and European Association of Geoscientists and Engineers and John Wiley & Sons Ltd.

pervasive. Basin configuration and depositional environment exerted additional control on chlorite distribution. In the confined turbidite system (e.g. Duva field), chlorite is typically found as coating, whereas in less confined turbidite systems (e.g. Agat field) chlorite shows complex distribution related to depositional environment and dewatering processes. Our findings demonstrate the importance of considering the entire sediment routing system, from source to sink, when predicting chlorite occurrence and its impact on reservoir quality in deep marine settings. This integrated approach can guide exploration and development efforts in deepwater clastic reservoirs.

KEYWORDS

chemical weathering, chlorite, Lower Cretaceous, North Sea, reservoir quality, sediment provenance, source-to-sink, turbidite

1 | INTRODUCTION

In many sedimentary basins, deeply buried sandstone reservoirs (>3500 m) are considered high-risk targets for geological exploration activities including hydrocarbon exploration, geothermal activity, or CO₂ storage. At such burial depths, quartz cementation is expected to severely reduce the reservoir properties (Giles et al., 1992). However, over the past years, several studies have reported well-preserved reservoir quality in deeply buried clastic reservoirs, related to the presence of chlorite coats around detrital grains (Azzam et al., 2022; Bloch et al., 2002; Ehrenberg, 1993; Saïag et al., 2016; Worden et al., 2020). Chlorite coats can preserve porosity by limiting quartz overgrowth (Ajdukiewicz & Larese, 2012; Azzam et al., 2022; Billault et al., 2003; Bloch et al., 2002; Ehrenberg, 1993; Saïag et al., 2016). Therefore, understanding the parameters that control chlorite coatings in sedimentary basins is crucial to predicting the quality of deeply buried reservoirs.

Chlorite is mainly authigenic in siliciclastic rocks, resulting from the replacement of early clay precursors such as berthierine, odinite, kaolinite, dioctahedral-smectite and trioctahedral-smectite (saponite for Mg-chlorites) (Azzam et al., 2022; Beaufort et al., 2015; Ryan & Hillier, 2002; Virolle et al., 2022). According to Dowe et al. (2012), the occurrence of chlorite in clastic reservoirs can be favoured under some particular geological settings and depositional environments: (1) chlorite-bearing reservoirs are more frequent in sediments derived from mafic igneous provinces and mixed provinces. This is because chlorite is rich in Fe and Mg, which requires a bedrock rich in Ferro-magnesian minerals (Worden et al., 2020). (2) Intense chemical weathering in tropical or temperate climates is important for chlorite development since it promotes the dissolution of Fe-Mg minerals in the

Highlights

- The development of chlorite in North Sea turbidites is strongly influenced by the sediment's provenance and the weathering conditions.
- Mixed source rocks with both mafic and felsic compositions promote the development of thick chlorite coats that reduce porosity.
- Differences in sediment provenance can result in significant variation in chlorite content over relatively short distances, with both positive and negative implications.
- Global climatic and tectonic activities during the Lower Cretaceous played a crucial role in the widespread chlorite development across Northern Europe.

bedrock and thus the amount of Fe and Mg transported by rivers (Azzam et al., 2022; Virolle et al., 2022). (3) Fe-chlorite precursor phases, such as odinite, berthierine, Fe-ooids, and glauconite, commonly develop in shallow marine environments due to the flocculation of suspended Fe-rich particles near river mouths (Azzam et al., 2022; Dowe et al., 2012; Ehrenberg, 1993; Griffiths et al., 2021; Odin, 1988). Additionally, the presence of biofilms produced by biological activity (particularly in estuarine settings) can help the adherence of detrital clays to the grains allowing good coverage by clay coating during transport or diagenesis (Duteil et al., 2020; Saïag et al., 2016; Virolle et al., 2019; Wooldridge et al., 2017). (4) High sea level periods, allow long residence time of the sediments on the shelf, hence promoting a strong accumulation of Fe-rich clay phases (Morad et al., 2013; Odin, 1988; Van Houten & Purucker, 1984). Other important conditions for Fe-rich

chlorite formation are the redox conditions during transport, sedimentation, and diagenesis, the presence of organic matter, and dewatering processes. Fe-rich chlorite may be abundant in poorly to moderately rich organic matter sandstone with low sulphate content. Siderite and pyrite will trap dissolved iron at the expense of Fe-rich clays if the sediments are rich in organic matter and if there is a prolonged interaction with SO₄-rich seawater (Azzam et al., 2022; Worden et al., 2020). Finally, dewatering processes can redistribute evenly the clay fraction within the sediment, allowing the formation of well-continuous chlorite coatings (Porten et al., 2019).

Most of the research work during the last years has focused on the mechanism of chlorite formation during diagenesis. However, there has been a lack of studies on how chlorite emplacement can be linked to sediment routing systems, which involve understanding the role of the source, climate, transport conditions and depositional environment. Therefore, integrated models for chlorite emplacement in sedimentary basins would be crucial to predicting the quality of deeply buried reservoirs. This paper aims to provide a source-to-sink model for Fe-rich chlorite formation in sedimentary basins. To do so, we focused on the Agat Formation (Fm) in the Northern North Sea. The Agat Fm consists of deep-sea channelised fan sediments deposited at the base of the shelf break of the Norwegian platform during the Aptian–Albian period (Martinsen et al., 2005). Previous petrographic studies have shown that chlorite plays a major role in controlling the quality of the reservoirs in the Agat Fm. It can have a positive impact by inhibiting quartz overgrowth, but it can also have a negative impact by blocking porosity and reducing permeability, with thick chlorite coats or pore-filling chlorites (Azzam et al., 2022; Hansen et al., 2021). The distribution of chlorite varies significantly throughout the Agat Formation. In the Duva field, located in the southern part of the Agat system (Block 36/7), chlorite can reach up to 25% of the total rock volume (Azzam et al., 2022). However, in the northern part, in the Agat field (block 35/3), the sandstone contains much less chlorite, ranging from 2% to 10% (Azzam et al., 2023). Moreover, the sandstone composition, texture, and sedimentary facies vary significantly between the two fields, indicating changes in the sediment routing. Therefore, the Agat Fm provides an excellent opportunity to examine the impact of the sediment routing system on chlorite development in siliciclastic rocks.

The main objectives of this study are to:

1. Identify the provenance of sediments and the paleoclimate conditions during the Lower Cretaceous.
2. Identify the impact of the sediment source composition, chemical weathering and depositional environment on chlorite development in sedimentary basins.
3. Determine the optimal conditions for chlorite development in sedimentary basins required for the preservation of reservoir quality.

Addressing these objectives will help identify new hotspot areas or geological periods that are prominent for chlorite development in sedimentary basins. This will provide important insights into predicting chlorite coat emplacement, helping to identify siliciclastic reservoirs even deeply buried.

2 | GEOLOGICAL SETTINGS

The study area is located in the Northern North Sea, on the Måløy slope bounded to the east by the Øy garden Fault Complex (N-S-striking normal faults) and to the west by the normal fault of the eastern margin of the Sogn Graben (Figure 1a). It comprises the Agat field in the north (block 35/3) and the Duva field in the south (block 36/7) (Figure 1b). The Agat Fm was first discovered in 1976 by Saga Petroleum, who found hydrocarbons in the Lower Cretaceous sandstone in block 35/3 (currently called the Agat field). Recently, Neptune Energy made significant oil and gas discoveries in 2017 in block 36/7, currently called the Duva field. A new discovery was made in 2022 in the Hamlet structure in block 35/9, with an estimated gross 2P reserves of more than 130 million barrels of oil equivalent, which confirms the ongoing potential of the Agat play.

The Agat Fm records progressive filling of early post-rift, intraslope relief, which was created following the major rifting phase of the Middle to Late Jurassic (Glennie, 2009) (Figure 1b). Rifting took place along large N-S and NE–SW trending normal faults, resulting in a horst and graben landscape dominated by eastward tilted fault blocks. Sedimentation during the early Cretaceous was dominated by fine-grained lithologies (marls and mudstone) recording an overall transgression (Figure 1c). However, this period was intruded by many regressive events interpreted to be related to the Austrian tectonic phase, which caused the rejuvenation of older landmasses during Aptian and Albian times (Bugge et al., 2001; Oakman & Partington, 1998; Ziegler, 1975, 1990). These events locally resulted in the remobilisation and progradation of siliciclastic sediments in deep sub-basins. In the Måløy Slope, this has created a deep-water sandstone system that constitutes the Agat Formation (Bugge et al., 2001; Jackson et al., 2008; Skibeli et al., 1995). The architecture and morphology of the

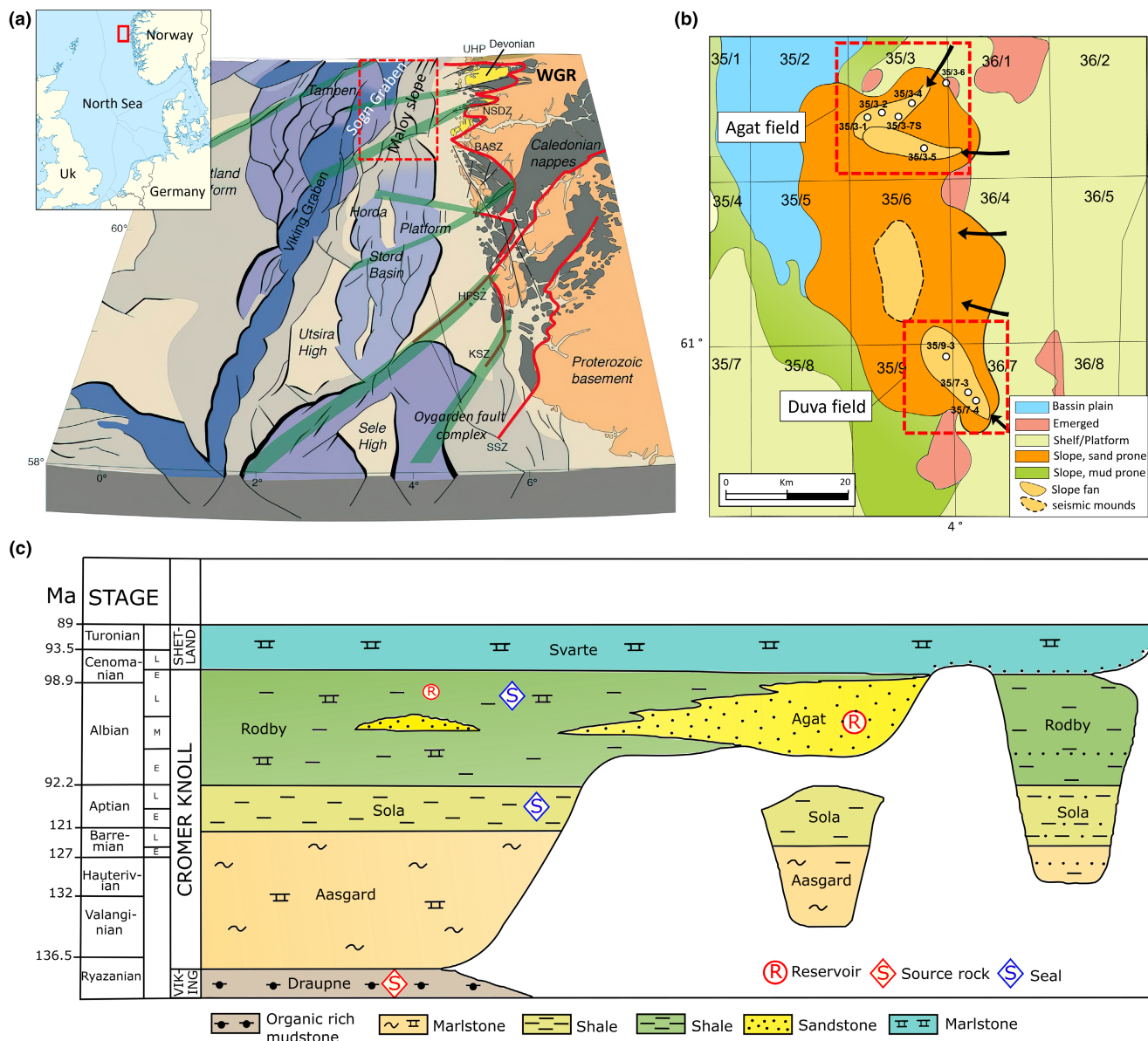


FIGURE 1 (a) Structural configuration of the Northern North Sea showing the main structural elements and major faults in the Study Area (from <https://folk.uib.no/nglhe/multirift.html> published with the authorisation of the author). The red lines and the green lines represent the shear zones and their offshore extension, respectively. NSDZ, Nordfjord-Sogn Detachment Zone; BASZ, Bergen Arc Shear Zone; WGR, Western Gneiss Region; ØC, Øygarden Complex (gneiss); ØFS, Øygarden Fault System; HSZ, KSZ, and, SSZ: Hardangerfjord, Karmøy, and Stavanger shear zones, respectively; (b) Palaeogeographical settings of the Agat Fm during the Albian-Aptian period showing the location of the two slope fan systems: Agat field in the north and the Duva field in the south (map modified from Gradstein et al., 2016); (c) East-West cross section showing the Lower Cretaceous stratigraphy of the Northern North Sea (Gradstein et al., 2016).

turbidite systems were mainly controlled by the complex topography of the inherited post-rift landscape (Martinsen et al., 2005). The sand intervals were deposited in a series of channel-levee and intraslope lobe systems in deep water, continental slope environment (Figure 1b) (Martinsen et al., 2005). Paleobathymetric reconstruction of the Måløy slope during the Aptian–Albian times suggests that the turbidite systems were sourced from the east, from a relatively small area (5000–8000 km²), and the adjacent paleo-shelf

was relatively narrow (20–30 km wide) (Bugge et al., 2001; Hansen et al., 2021; Jackson et al., 2008; Martinsen et al., 2005).

2.1 | Lithostratigraphy

Owing to the complex topography of the slope system during the Lower Cretaceous, the Agat Formation was formed

under varying depositional environments and was probably supplied from different small source areas (Gradstein et al., 2016). Previous studies by Azzam et al. (2022, 2023) indicated a strong variation in the depositional environment between the Agat and Duva fields, which led to a high degree of heterogeneity in reservoir quality in the Agat Fm. The following section provides an overview of the depositional environments in both the Agat and Duva fields.

2.1.1 | The Duva field

The Duva turbidite system is defined by its thick, massive, and largely structureless sandstone units that have been entirely cored in well 36/7-4 (Azzam et al., 2022; Hansen et al., 2021) (Figure 2). The sediments were supplied from the remobilisation and reworking of shelf-derived shallow marine sands (Azzam et al., 2022; Hansen et al., 2021). The sediments were deposited within a deeply incised channel complex that was approximately 50 m deep and

3 km wide according to 3D seismic data (Neptune energy internal communication). Such structural confinement in the Duva field has resulted in the deposition of a homogeneous sandstone succession.

Despite the homogeneous, structureless character of the Duva sands, there is a significant change in sediment composition and reservoir quality between the upper part and lower part of the turbidite system. In the upper part (hereafter called Upper Reservoir—[UR]), the sandstone is dominated by quartz, contains only small amounts of clay materials, and displays excellent reservoir quality. In the lower part (hereafter called Lower Reservoir—[LR]), the sandstone is highly rich in green clay materials (mainly chlorite), which strongly reduces the reservoir quality (Azzam et al., 2022). According to seismic data, the UR is more laterally extensive than the LR (Neptune energy internal communication) (Figure 2). The LR interval extends about 3 km into the basin beyond the 36/7-3 well, where it downlaps onto the basin floor, whereas the UR extends almost as far as the 35/9-3 T2 well (Figure 2).

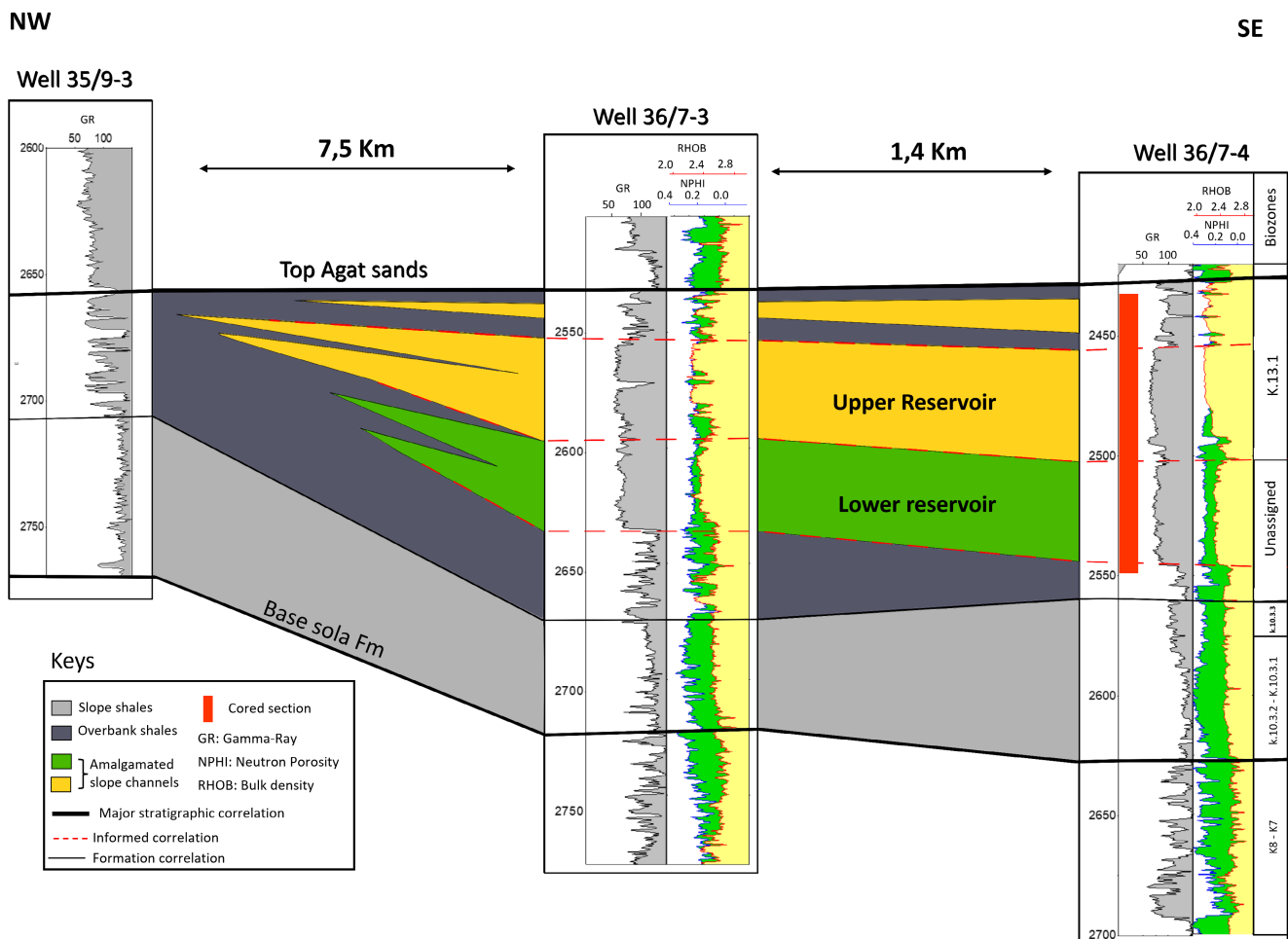


FIGURE 2 NW-SE correlation between wells 35/9-3 T2, 36/7-3 and 36/7-4 in the Duva field. Two reservoirs are distinguished: an upper clean reservoir and a lower clay-rich reservoir (well logs data are provided by Neptune Energy).

2.1.2 | The Agat field

Sandstone in the Agat field shows more complex sedimentary facies distribution with strong vertical heterogeneity compared to the massive turbidite system in the Duva field (Azzam et al., 2023; Lien et al., 2006). Based on the core description, well logs response, and biozones, the turbidite system in the Agat field has been subdivided into five members (Agat 50, 60, 70, 80, and 100) (VNG Norge internal report) (Figure 3). The Agat 50 interval is composed of overbank mudstone and interbedded banded sandstone, interpreted as a distal deepwater lobe system. The Agat 60 is dominated by the deposition of fine-grained sediments (siltstone and mudstone) reflecting a period of regional sea-level highstand. The Agat 70 interval is composed of high Net-to-Gross amalgamated sands, interpreted as a lobe complex. The transition from Agat 70 to Agat 80 is composed of siltstones-mudstone, injected sandstones, deformed units, and debrites, indicative of a distal setting and system backstepping. The Agat 80 is dominantly composed of stratified sand units, interpreted as a weakly

confined channelised succession. Finally, the Agat 100 is composed of medium-grained sandstone in the South and fine-grained in the North, interpreted as a channel complex and a levee deposit, respectively. The complex architecture of the turbidite system in the Agat field may reflect the poorly confined nature of the slope fan, which allowed lateral migration and avulsion of channels resulting in marked vertical heterogeneity.

3 | METHODS

3.1 | Petrography

A Leica DM750P polarising microscope was used to observe thin sections under different magnifications. A composite microphotograph was created from a set of overlapping images for each thin section and then point-counted 250 times using Jmicrovision® software (Roudit, 2007). Additionally, the size of approximately 300 grains was measured along their longer axis. Data

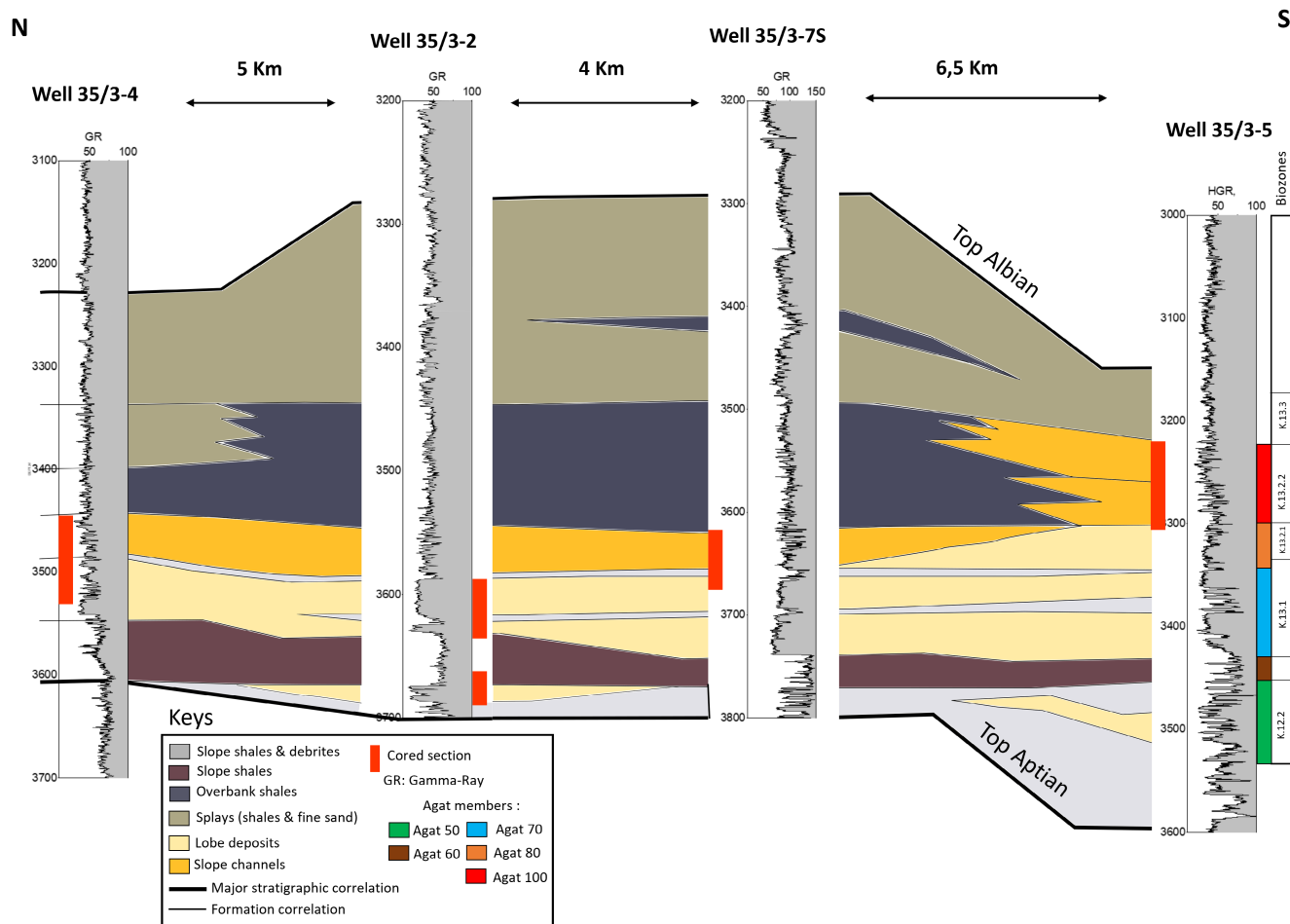


FIGURE 3 N-S stratigraphic correlation of deepwater sub-environments in the Agat 50 to Agat 100 interval in the Agat field, based on core sedimentology and gamma-ray response (modified from VNG Norge internal report).

were then imported to Gradistat © Simon Blott, a software calculating the grain size distribution, skewness, and sorting (Blott & Pye, 2001). Sphericity and roundness were visually defined following the chart of Krumbein (1963).

3.2 | Bulk rock chemistry

Fifty bulk rock samples were analysed for major, minor, and trace elements at the ALS Minerals laboratory located in Loughrea, Ireland. The samples were first crushed and split before being shipped to the laboratory for analysis. Major element chemistry was determined through XRF analysis of lithium borate fused beads, while trace and rare earth elements were measured through ICP-MS on lithium borate fused samples that were dissolved in a four-acid mixture of HF, HNO₃, HCl and HClO₄. The total carbon and sulphur content were measured through infrared combustion (LECO) analysis.

3.3 | Heavy minerals

Twenty-five samples were selected for heavy minerals (HMs) analysis. Samples have been crushed and sieved in two series of metal sieves with a mesh size of 400 and 63 µm. The grain size fraction between 63 and 400 µm was selected based on petrographic observation, which shows that most of the heavy minerals are between 65 and 400 µm in size. HMs were then separated using bromoform. The extracted fraction was then subjected to magnetic separation to eliminate undesired heavy minerals (chlorite, glauconite, siderite) using a Frantz magnetic separator. The recovered HM fraction and homogeneously distributed on a watch glass. For each sample, at least 300 grains are mounted in resin blocks. Resin mounts are then polished and analysed using FTIR spectroscopy. The instrument used to quantify heavy minerals is a PerkinElmer FTIR Microscope Spotlight 400 available at the Geosciences Paris-Saclay (GEOPS) laboratory. The spectra were obtained in reflectance mode in the range 4000 to 550 cm⁻¹, with a resolution of 4 cm⁻¹, with an interval of 1 cm⁻¹, and with 25 scans at 20°C. Analysis was made using point mode with a spatial resolution of 20 µm. The quantification of heavy minerals is made using in-house software “Quanti HM” written in Julia, which establishes a correlation coefficient between the infrared spectrum of the analysed mineral and the database. The results of quantification are calculated as a function of a user-selected minimum correlation coefficient, which varies among samples between 75% and 90%.

3.4 | Zircon U–Pb geochronology and garnet geochemistry

Zircon crystals of varying sizes between 80 and 400 µm were handpicked, mounted in epoxy, and polished to expose their surface for laser ablation. The morphological parameters of zircons (length, width, elongation, surface) were measured using Jmicrovision® software. The mounts were examined using cathodoluminescence microscopy (OPEA cathodyne 12–15 keV, 150–200 mA) before their ablation. Zircon U–Pb geochronology was performed at the GEOPS laboratory using a sector field inductively coupled plasma mass spectrometer coupled to a laser ablation system (LA-SF-ICP-MS). The laser ablation system was operated at a repetition rate of 10 Hz with an ablation time of 30 s, a spot size of 35 µm, and a fluence of 3 J cm⁻². Calibration for the zircon analyses was carried out using the geostandard 91500 zircon, which was probed every 15 analyses. Quality control was achieved for most samples using the Plesovice standard. The obtained U–Pb age of the 91500 zircon was 1063 ± 10 Ma, with a total of 80 analyses, and 337 ± 4 Ma for the Plesovice zircon, with a total of 92 analyses. The data reduction was performed using the iolite 3 software package by filtering the time-resolved signal to remove disturbed ratios. The resulting plots were generated using the IsoplotR software (Vermeesch, 2018), following the concordant age treatment of Ludwig (1998). For more details on the U/Pb zircon methodology, please refer to the supplementary materials.

Garnet crystals ranging between 80 and 400 µm in size were handpicked, mounted in resin, and polished to expose their surface for Scanning electron microscopy (SEM) analysis. Garnet major elemental composition is measured using a Phenom mini-SEM benchtop (10 keV in imaging mode and 15 keV for elementary analyses) equipped with an Energy-Dispersive X-ray spectroscopy analyser (GEOPS laboratory).

4 | RESULTS

4.1 | Textural and mineralogical comparison between the Duva and Agat field

4.1.1 | Detrital mineralogy—Rigid framework

The Duva and Agat fields exhibit distinct textural characteristics (Figure 4a,b). The Duva field is characterised by medium to coarse-grained sandstone (ranging from 270 to 550 µm), locally pebbly, that is overall poorly to moderately sorted. The Agat field features finer sands (<250 µm)

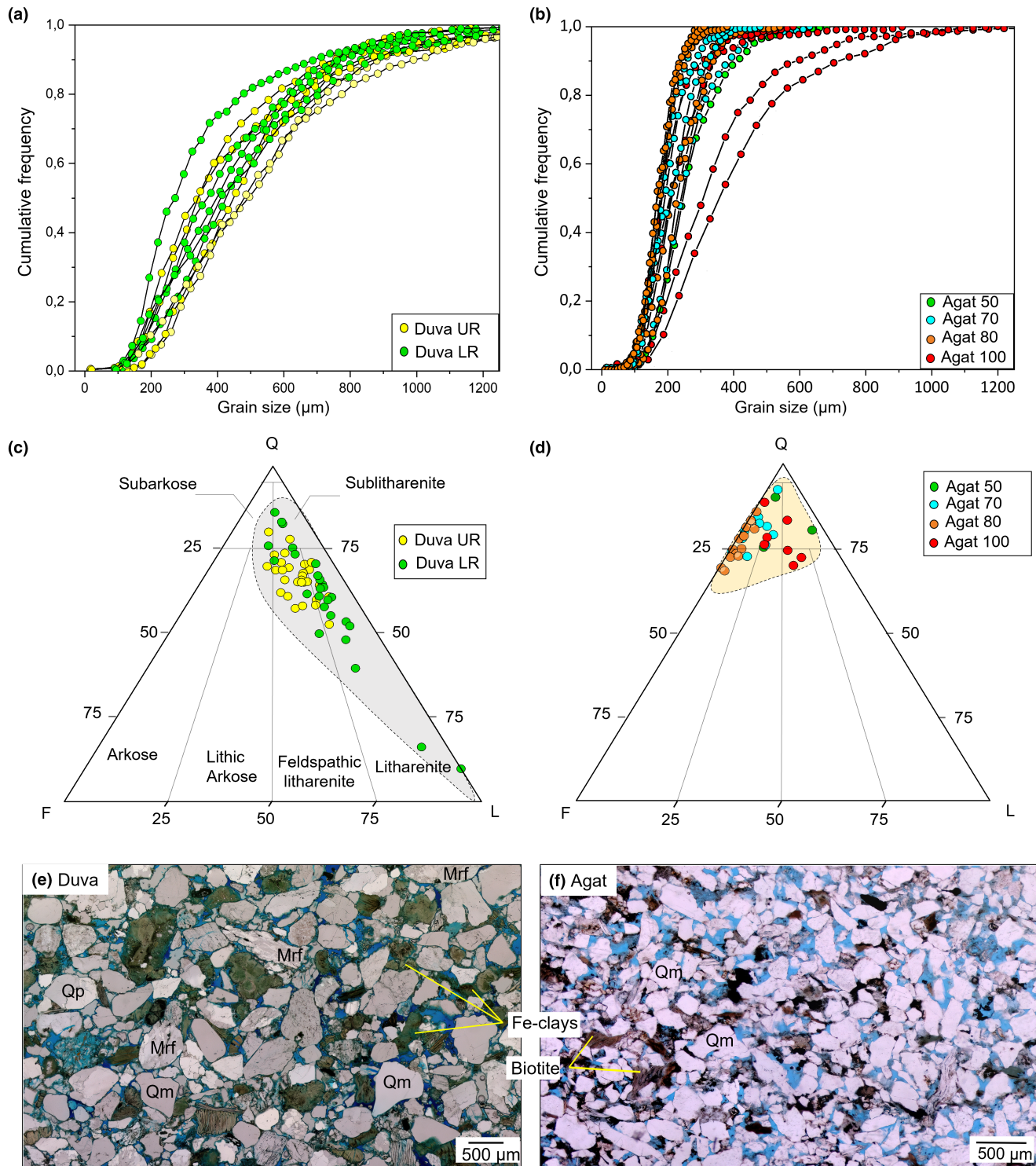


FIGURE 4 (a, b) Cumulative grain size frequency for sandstone in the Duva field and the main Agat members in the Agat field; (c, d) QFL (Quartz–Feldspar– Lithics) ternary diagram of the sandstone population in the Duva field and the Agat field; (e) mineralogical assembly from the Duva field showing sandstone that is coarse-grained and poorly sorted. Grains are composed of polycrystalline (Qp), monocrystalline quartz (Qm) and K-feldspar, with a wide distribution of metamorphic rock fragments (Mrf). Note the presence of a high amount of green clays (Glaucanite and Fe-illite); (f) mineralogical assembly from the Agat field showing fine-grained sandstone that is well sorted. Sand grains are mostly monocrystalline. Note the presence of biotite and the absence of green clays.

that are generally well sorted, except for the Agat 100 unit, which contains poorly sorted, medium-grained sandstone.

Table 1 illustrates the average mineralogical composition of the different sandstone units in the Agat Fm, including detrital and authigenic minerals.

Sandstone in the Duva field is mainly classified as litharenite to feldspathic litharenite sandstone, showing a high proportion of metamorphic lithic fragments (av. 13%) (Figure 4c,e). Quartz grains are mainly monocrystalline quartz (av. 23%) with subordinate polycrystalline quartz (av. 10%), many of which show undulose extinction under cross-polarised light. Feldspar is mainly composed of orthoclase and microcline, with traces of plagioclase (av. 0.5%). The UR has an average of 7% of K-feldspar, while the LR has an average of 3.4%.

On the other hand, the Agat field mainly consists of subarkosic and arkosic sandstone (Figure 4d,f), with some samples falling into the feldspathic litharenite domain. Monocrystalline quartz is the most abundant mineral, ranging from 35% to 46%, with polycrystalline quartz ranging from 9% to 18% (Figure 4f). Lithic fragments are present in small amounts, averaging around 3%, except for the Agat 100 unit, which has a higher proportion of metamorphic fragments (av. 7%). The percentage of feldspar varies significantly in the Agat field, with the Agat 80 unit having the highest percentage (av. 13%), followed by the Agat 70 unit (av. 10%), and the Agat 100 unit (av. 7%), and

the Agat 50 unit having the lowest percentage at less than 5%. Plagioclase is ubiquitous in the Agat field, with the Agat 50 and Agat 70 units being dominated by plagioclase and the Agat 80 and Agat 100 units primarily composed of K-feldspars.

Overall, the Duva field is characterised by coarser grain size and higher concentration of metamorphic lithic fragments, while the Agat field is characterised by finer grain size and higher concentration of monocrystalline quartz and feldspars (both K- and Na-rich feldspars) with a relatively low percentage of lithic fragments.

4.1.2 | Ductile framework and Fe-bearing detrital grains

The ductile framework in the Agat Fm is mainly composed of Fe-bearing grains, which include glauconite, ferric illite (Fe-illite), biotite and pseudo-matrix. Pseudo-matrix includes some degraded igneous lithic fragments (volcanic fragments) and a mixed clay matrix composed of Fe-bearing kaolinite and Hydroxy-interlayered minerals (HIMs) mixed with illite. Fe-poor grains like muscovite are present in small amounts.

The distinction between glauconite and ferric illite is based on the studies of Azzam et al. (2022) and Patrier et al. (2023), who differentiated the various green minerals

TABLE 1 Average mineralogical composition of the different sandstone intervals in the Agat Fm.

Mineralogy	Duva UR	Duva LR	Agat 50	Agat 70	Agat 80	Agat 100
Mo quartz	26.7	21.8	34.3	45.2	41.9	32.4
Po quartz	13	10.1	18.8	9.6	10.2	18.2
K-feldspar	6.1	2.9	1.4	5.7	10	5.2
Plagioclase	0.9	0.6	3.7	5.3	3.2	2.1
Lithic fragments	13.1	16.4	6	1.9	2	7.3
Glauconite pellets	4.5	6.9	0.2	1.7	1.3	1.6
Ferric illite	4.9	7.8	0.7	1	1.3	1
Biotite	0.2	0	7.4	3.4	3.3	3.7
Muscovite	0.5	0.3	2.3	1	1.9	0.7
Pseudomatrix	4.8	9.3	0	1.1	3.4	4.5
Authigenic mineralogy						
Quartz overgrowth	0.5	0.2	4.4	1.5	0.4	1
Chlorite coating	4.9	15.2	2.4	2.4	3	1.6
Porefilling chlorite	0	0	10.3	2.1	2	5.3
Siderite	1.6	2.6	8.2	0.8	0.4	3.6
Kaolinite	0	0	3.2	2.7	1.6	1.5
Apatite	0.5	0.4	0	0	0	0
Calcite	1.3	2	0.3	5.4	13.4	6.3
Porosity	16.5	3.5	0	9.2	0.7	4

in the Agat Fm based on their chemistry and morphology. By definition, iron in glauconite occurs in both ferric and ferrous states, while it is mainly ferric in Fe-illite (Patrier et al., 2023). The latter generally occurs as long vermicular pellets (Figure 5b,c), which resemble biotite under cross-polarised light. Glauconite, on the other hand, shows a more globular massive shape and is generally opaque under cross-polarised light (Figure 5b,c,g). Biotite is distinguished by its dark brownish colour, forming elongated crystals (Figure 5f) with moderate to strong pleochroism. Muscovite appears as tabular or elongated crystals that are distinguished from biotite by its pale silvery-white colour. Pseudo-matrix consists mainly of Fe-bearing volcanic fragments, which have undergone strong compaction, containing residues of mica, feldspar and silt-size quartz (Figure 5c). In the Agat field, pseudo-matrix mainly comprises detrital Fe-bearing kaolinite and mixed-layer clay minerals (MLM) composed of HIMs and illite. According to Azzam et al. (2023), these clays have a pedogenetic origin.

The percentage of Fe-bearing minerals varies significantly between the Agat and the Duva fields. Glauconitic materials, Fe-illite, and pseudomatrix are widely distributed in the Duva field. The LR in the Duva field contains a higher percentage of glauconite pellets (av. 6.9%) and Fe-illite (av. 7.8%), compared to the UR (4.5% and 4.9%, respectively). Similarly, the percentage of pseudomatrix is also higher in the LR (9.3%) compared to the upper reservoir (av. 4.8%). It is noteworthy that pseudomatrix, despite having a detrital origin, is generally totally replaced by chlorite in the Duva field. Figure 5d shows some relics of detrital kaolinite in pseudo-matrix that have been completely replaced by chlorite (only the vermiform morphology of kaolinite can be distinguished). Biotite and muscovite are present in trace amounts in the UR, with an average of 0.2% and 0.5%, respectively, and are nearly absent in the LR. Fe-grains in the Duva field are generally associated with phosphatic concretions, which according to Azzam et al. (2022), indicate that they formed in shallow marine environments.

The Agat field has a lower percentage of glauconitic materials (ranging from 0.2% to 1.7%) and ferric illite (ranging from 0.7% to 1.3%) across all units (Figure 5e). Biotite is present in higher amounts in the Agat field, with

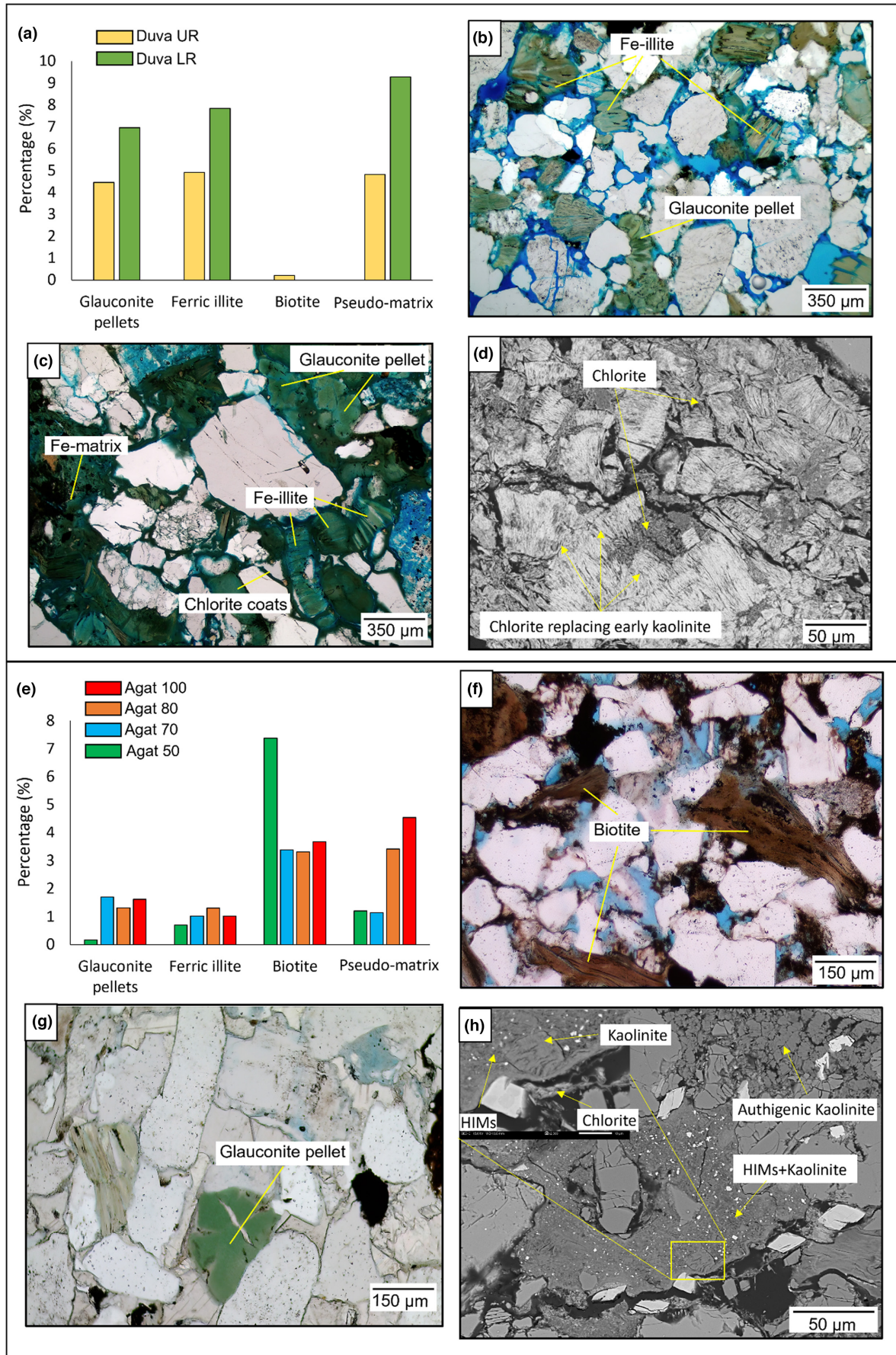
the highest percentage found in the Agat 50 unit (av.7.4%) and is close to 3.5% in the other units (Agat 70, Agat 80, and Agat 100) (Figure 5d). Muscovite is present in a lower proportion than biotite (ranging from 1.0% to 2.3%). Pseudomatrix in the Agat field includes detrital kaolinite, and mixed layer clays composed of Fe-bearing kaolinite, HIMs, and illite (Figure 5h). Pseudo-matrix is present in a minor amount in Agat 50 and Agat 70 (Traces up to 2%) but is relatively high in Agat 100 (av. 4.5%) and Agat 80 (av. 3.4%).

4.1.3 | Chlorite in the Agat Formation

Chlorite, kaolinite, siderite, pyrite, quartz overgrowth and calcite are the main authigenic minerals in the Agat Fm. Chlorite is the most important authigenic mineral since its presence plays a crucial role in determining the reservoir quality of the Agat Fm. Its presence and configuration in the sandstone can positively or negatively impact the reservoir quality, leading to the division of the Agat Fm into different groups (Figure 6a):

1. Group 1 shows the highest reservoir quality, characterised by porosity greater than 15% and permeability that varies between 500mD and up to 12,000mD. This group is characterised by low amounts of chlorite forming thin coats that completely cover detrital grains (Figure 6b) associated with extensive dissolution of feldspar grains. This group mainly forms the UR in the Duva field.
2. Group 2 is characterised by porosity between 7% and 15% and permeability between 100 and 1000mD. Chlorite in this group shows similar characteristics to group 1 forming a thin continuous coating around detrital grains. However, this group is characterised by a higher amount of kaolinite due to the extensive dissolution of feldspar in a closed diagenetic system (Figure 6c). This group mainly forms the lobe deposits of Agat 70 and the channel complex of Agat 80 in the Agat field.
3. Group 3 is characterised by porosity between 1 and 10% and permeability between 3 and 75mD. This group is characterised by sandstone with thick chlorite coats

FIGURE 5 (a) Fe-bearing mineral composition in the Duva field; (b) photomicrograph of Fe-bearing Minerals in the UR of the Duva Field. It highlights the widespread occurrence of glauconitic grains and vermicular Fe-illite; (c) photomicrograph of the LR in the Duva Field. This image displays a sandstone predominantly composed of glauconite and vermicular Fe-illite. These elements are partially to completely replaced by chlorite. (d) SEM image showing chlorite completely replacing kaolinite and pseudo-matrix in the Duva field; (e) Fe-bearing mineral composition in the Agat field; (f) photomicrograph of Fe-bearing Minerals in the Agat Field, displaying the common presence of biotite; (g) rare occurrence of glauconite in the Agat Field, appearing as isolated grains with massive globular morphology; (h) SEM image of pseudo-matrix in the Agat field, which consists of kaolinite and Hydroxy-interlayered clay minerals (HIMs). Note that chlorite only replaces the outer part of the pseudo-matrix.



- which can reach up to 30 μm in size, significantly reducing the permeability of the sandstone (Figure 6d). This group typically forms the LR in the Duva field.
- Group 4 shows similar reservoir quality to Group 3: chlorite in this group is mainly found as a pore-filling mineral, significantly reducing permeability (Figure 6e). Group 4 is generally related to distal lobe deposits of the Agat 50 and the channel and levee deposits of the Agat 100.
 - Group 5 is characterised by porosity of less than 7% and permeability between 0.5 and 75 mD. It comprises samples with thin discontinuous chlorite coatings around detrital grains (clay-coat coverage <40%). The discontinuous character of these coats allowed extensive cementation by quartz, which reduced both porosity and permeability (Figure 6f). This group is detected in Agat 70 and Agat 50 composed of amalgamated lobe deposits and distal lobe deposits, respectively.
 - Group 6 shows the poorest reservoir quality due to extensive calcite cementation (Figure 6g). Calcite fills most of the pore space leaving some residual porosity. Calcite is not restricted to any units but widespread across the Agat Fm both in the Duva field and the Agat field.

Overall, the Agat reservoir quality is greatly affected by the presence of chlorite, mainly by the amount of chlorite in the pores and the thickness of the chlorite coats. Higher amounts of chlorite in the pores and thick coats result in lower reservoir quality that allows the development of quartz overgrowth. The reservoir quality is better preserved with thin continuous chlorite coats rather than a discontinuous coating. Additionally, the presence of other minerals such as kaolinite and calcite can also lower the reservoir quality.

4.2 | Whole rock chemistry

4.2.1 | Major and minor elements

The bulk chemistry of the Agat Fm is given in supplementary materials. A strong chemical variation is observed between the Duva field and the Agat field, as well as a significant deviation within the different reservoir units (Figure 7).

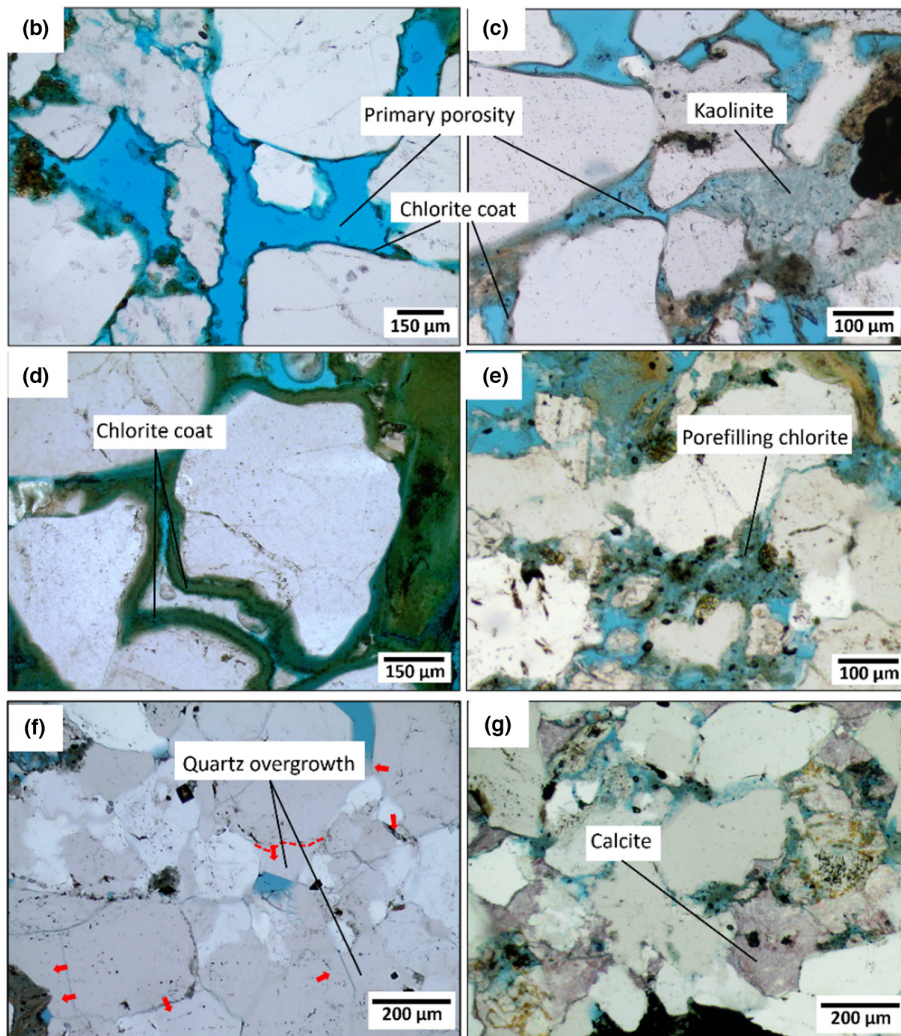
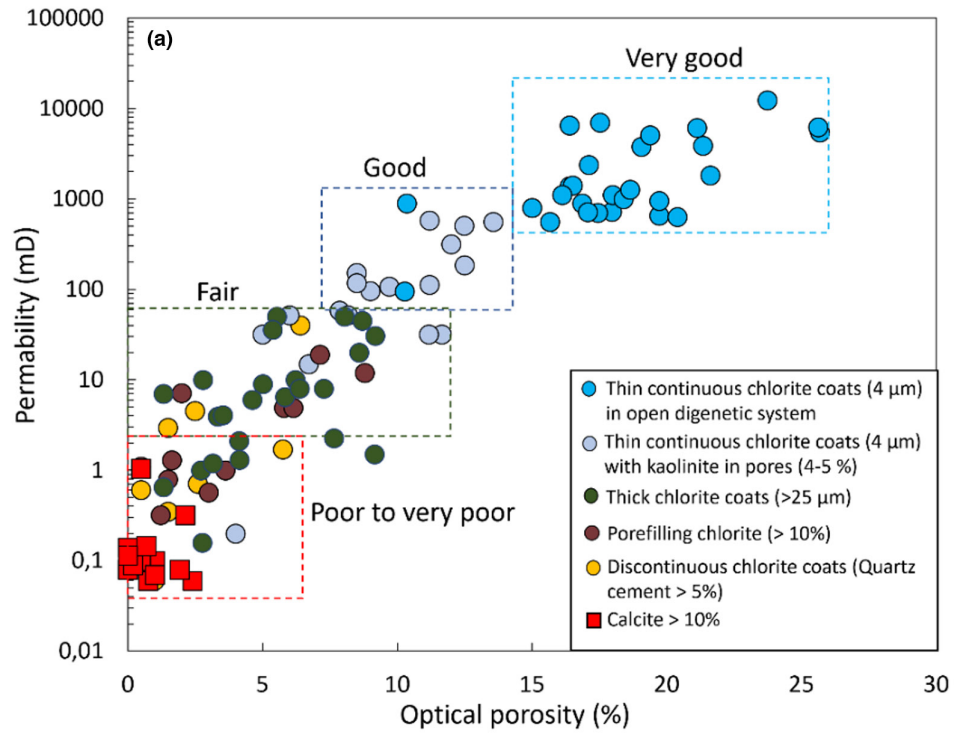
In the UR of the Duva field, the average SiO_2 , Al_2O_3 , Fe_2O_3 , CaO , K_2O , MgO content is 78.19%, 5.73%, 7.11%, 1.84%, 0.60%, 2.08%, 0.60%, respectively. The average content of minor elements such as Na_2O , TiO_2 , P_2O_5 , Cr_2O_3 , MnO is 0.34%, 0.34%, 0.17%, 0.01%, 0.06%, respectively. The average C (total carbon) content is 0.87% and the average loss on ignition (LOI) is 4.0%.

In the LR, the average SiO_2 , Al_2O_3 , Fe_2O_3 , CaO , K_2O , MgO content is 68.69%, 6.73%, 13.18%, 2.20%, 1.76%, 1.15%, respectively. The average content of minor elements is 0.38%, 0.43%, 0.23%, 0.01%, 0.08% for Na_2O , TiO_2 , P_2O_5 , Cr_2O_3 , MnO , respectively. The average LOI is 5.22%, and the average C content is 1.16%. Overall, the Lower Reservoir unit has a higher percentage of Fe_2O_3 , MgO and Al_2O_3 , while the Upper Reservoir unit has a higher percentage of SiO_2 and K_2O . The Lower Reservoir also has a higher percentage of LOI.

In the Agat field, the average SiO_2 , Al_2O_3 , Fe_2O_3 , CaO , K_2O and MgO is 76.97%, 5.47%, 3.08%, 5.20%, 1.32% and 0.62%, respectively. Minor elements have an average content of 0.66%, 0.76%, 0.05%, 0.003% and 0.08% for Na_2O , TiO_2 , P_2O_5 , Cr_2O_3 and MnO , respectively. The average C content is 1.48% and the average LOI is 5.87%. The Agat 50 unit has the highest percentage of SiO_2 (av. 85.85%), Fe_2O_3 (av. 3.96%), and Na_2O (av. 0.79%), while the Agat 100 unit has the highest percentage of CaO (av. 8.17%). The Agat 70 unit has the highest percentage of TiO_2 , with an average of 1.11%. The Agat 80 unit has the highest percentage of K_2O (av. 1.81%), MgO (av. 0.74%) and Al_2O_3 (av. 5.64%) compared to the other Agat units.

Figure 7 shows correlation diagrams of selected oxides in the Duva and Agat fields. The relationship between Al_2O_3 and SiO_2 is used to evaluate the shale content in the sandstone. Typically, there is a negative linear correlation between Al_2O_3 and SiO_2 , as the quartz content decreases, when the content of clay minerals increases (Craigie, 2018). The Agat field displays a slightly higher $\text{SiO}_2/\text{Al}_2\text{O}_3$ ratio, consistent with the higher amount of quartz in the Agat field. Fe_2O_3 and MgO show positive linear correlation but with distinct trends for the Agat and Duva fields. The highest concentrations of Fe_2O_3 and MgO are found in the Duva field in the LR, suggesting these elements are primarily associated with chlorite. Figure 7 shows a weak correlation between K_2O and Na_2O , but with a significant increase in Na_2O in the Agat field consistent with the higher amount of plagioclase.

FIGURE 6 (a) Cross-plot of permeability versus optical porosity illustrating the effect of chlorite on reservoir quality; (b) photomicrograph of the Upper Reservoir (UR) from the Duva field, exhibiting excellent reservoir quality with most of the sand grains covered with thin, continuous chlorite coats; (c) photomicrograph of the Agat field (Agat 80), displaying good reservoir quality with well-continuous thin chlorite coats, but with primary porosity filled by kaolinite; (d) photomicrograph of the Lower Reservoir (LR), displaying thick chlorite coats that block the connectivity of the pore network; (e) photomicrograph of chlorite filling the intergranular volume in the Agat field (Agat 50); (f) photomicrograph of a sample in the Agat field (Agat 70) dominated by quartz overgrowth and lacking chlorite coats; (g) photomicrograph of sample dominated by calcite.



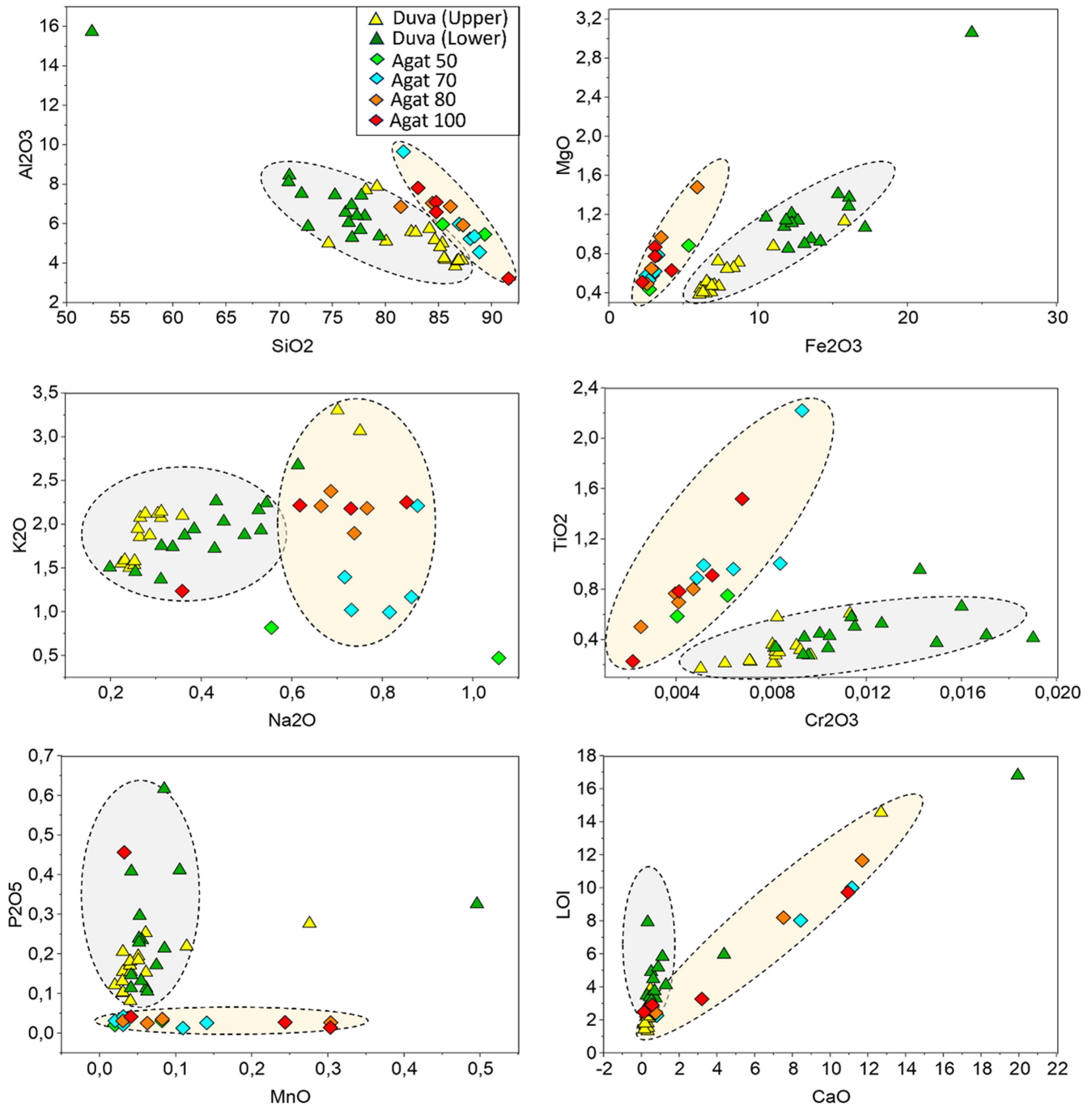


FIGURE 7 Cross-plots of major oxides showing distinctive trends between the Agat field and the Duva field (all units are in oxide wt.%).

TiO₂ and Cr₂O₃ display a positive linear correlation but with distinct trends between the Duva and Agat sandstones. TiO₂ and Cr₂O₃ are primarily associated with chromite and rutile, or other TiO₂ oxides (Craigie, 2018). TiO₂ shows a small variation in the Duva field, while Cr₂O₃ is highly enriched in the LR. In contrast, Cr₂O₃ varies slightly in the Agat field, but TiO₂ shows strong variation, with an enrichment in the Agat 70.

Figure 7 also shows a distinct trend of P₂O₅ and MnO, with higher concentrations of P₂O₅ in the Duva field and more MnO in the Agat field. The relatively high

concentration of P₂O₅ in the Duva field is consistent with its higher abundance in phosphate clasts and diagenetic apatite (Azzam et al., 2022). In contrast, higher manganese in the Agat field is found in calcite-cemented samples.

The relationship between LOI and CaO can be used to estimate the amount of carbonates, clays, and organic matter (Heiri et al., 2001). Only traces of organic matter are detected in the Agat Fm suggesting that LOI is primarily related to clays and carbonates, which explains the presence of two distinct trends. The increase of LOI in the Duva field, while CaO constant, is mainly due to

the presence of clays, particularly chlorite. The mutual increase of LOI with CaO is indicative of the presence of carbonates (calcite or siderite).

4.2.2 | Trace and rare earth elements

Trace and rare earth elements (REEs) geochemical data are normalised to the average values in the upper continental crust (UCC: Rudnick & Gao, 2003) and post-Archean Australian Shale (PAAS: Taylor & McLennan, 1985). UCC-normalised and PAAS-normalised distributions are illustrated in Figure 8a,b.

Figure 8a shows distinct UCC-normalised distributions between the Agat and Duva fields. It also shows some variability between the UR and the LR in the Duva field and slight variability within the Agat field reservoir units. Most trace elements in the UR are depleted relative to UCC, except Zr (av. 178 ppm), V (av. 80 ppm), and Li (av. 25 ppm). The LR shows a similar trend as the UR but is

more enriched in Zr (av. 191 ppm), V (av. 156 ppm), Ni (av. 31 ppm), Cr (av. 76 ppm), and Zn (av. 114 ppm).

The Agat Field shows strong depletion in all trace elements except for Zr (av. 625 ppm), Nb (av. 12 ppm), and Sr (av. 341 ppm) with the strongest enrichment in Zr being observed in Agat 70 reaching up to 2500 ppm. Overall, the Duva field is highly enriched in V, Ni, Cr, Zn and Cu relative to the Agat field. The latter shows strong enrichment in Zr and Sr.

In terms of REEs distribution (Figure 8b), the Duva field exhibits a PAAS-normalised pattern characterised by a light REEs (LREEs) enrichment relative to heavy REEs (HREEs), and strong positive Ce/Ce* anomaly, with an average of 1.32 in the UR and 1.57 in the LR. The average Eu/Eu* anomaly is 0.73 in the UR and 0.71 in the LR. The total rare earth elements (Σ REE) range from 53 ppm up to 201 ppm with an average of 96 ppm in the UR and an average of 133 ppm in the LR.

In the Agat field, the REE distributions show no fractionation between LREEs and HREEs except for some

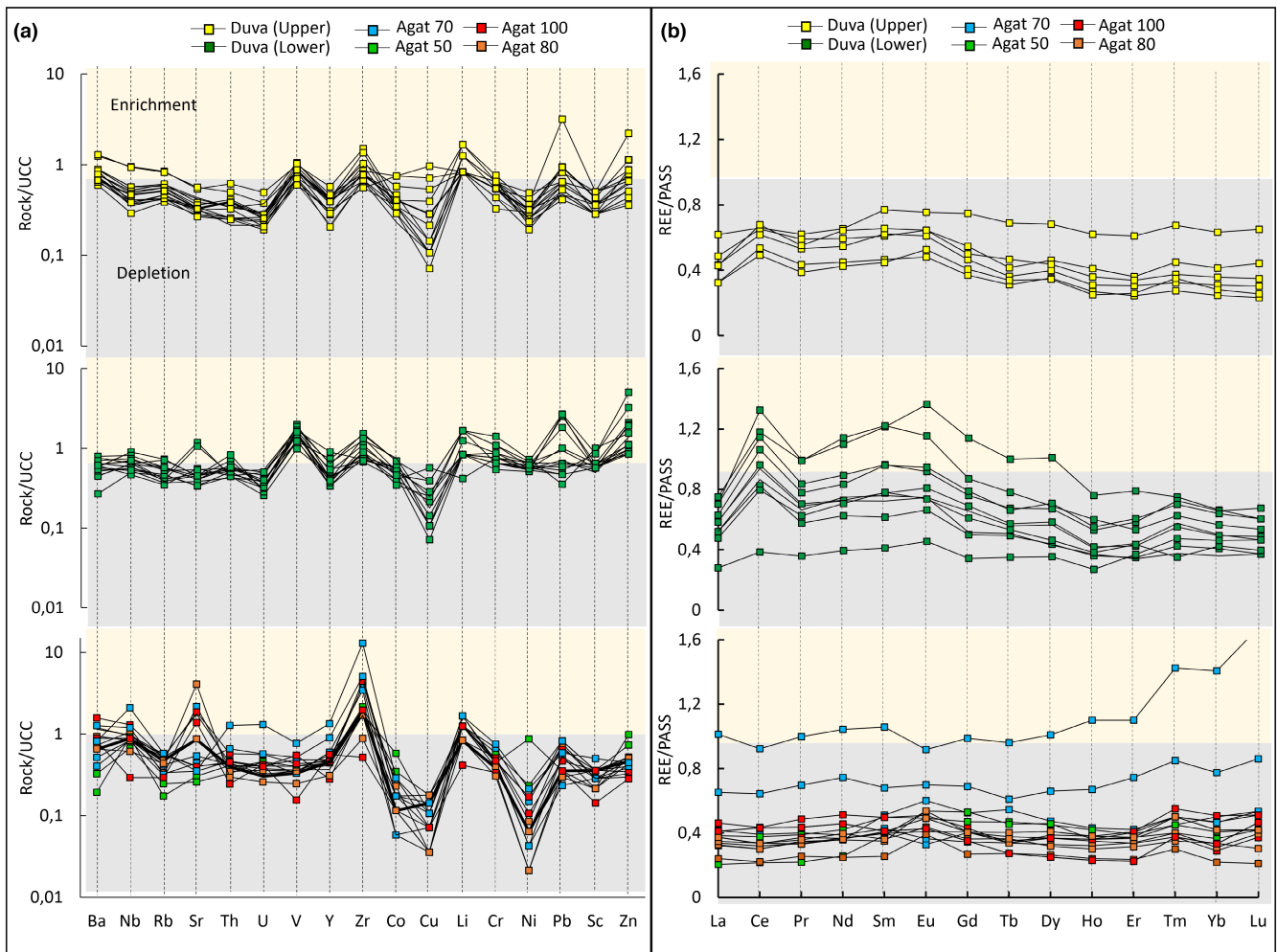


FIGURE 8 (a) UCC-normalised multi-element and (b) PASS-normalised REE plots of sandstone populations in the Agat Fm.

samples in the Agat 70 showing strong HREE enrichment. The Ce/Ce* anomaly is consistent in all Agat field units with an average of 1.01. The Eu/Eu* anomaly ranges from 0.62 up to 0.96 with an average of 0.75. The total rare earth elements (Σ REE) range from 43 ppm up to 180 ppm with an average of 76 ppm.

4.3 | Heavy minerals

The heavy mineral (HM) assemblages in the Agat Formation show low variations in both the Agat and the Duva fields. Overall, transparent HM assemblage is primarily composed of zircon and subordinate rutile and garnet. Other transparent HMs such as anatase, apatite,

and tourmaline are present in minor amounts and sporadically. Opaque minerals are mainly dominated by TiO₂ oxides (altered ilmenite) (Figure 9e,f), pyrite, chromite, amphibole (tremolite and actinolite) and biotite. Figure 10 shows the percentage of transparent HMs along with HM indices such as garnet: zircon index (GZi), rutile: zircon index (RuZi), and apatite: zircon index (AZi) and zircon morphology distribution (Morton & Hallsworth, 1994).

In the Duva field, transparent HMs is dominated by zircon which ranges from 48% up to 96%. However, a strong variation is noted in HM indices between the UR and the LR. The UR is characterised by high GZi and RuZi, and moderately high AZi. Conversely, the LR shows a significant downhole decrease of all indices showing dominant composition by zircon reflecting an ultra-stable composition.

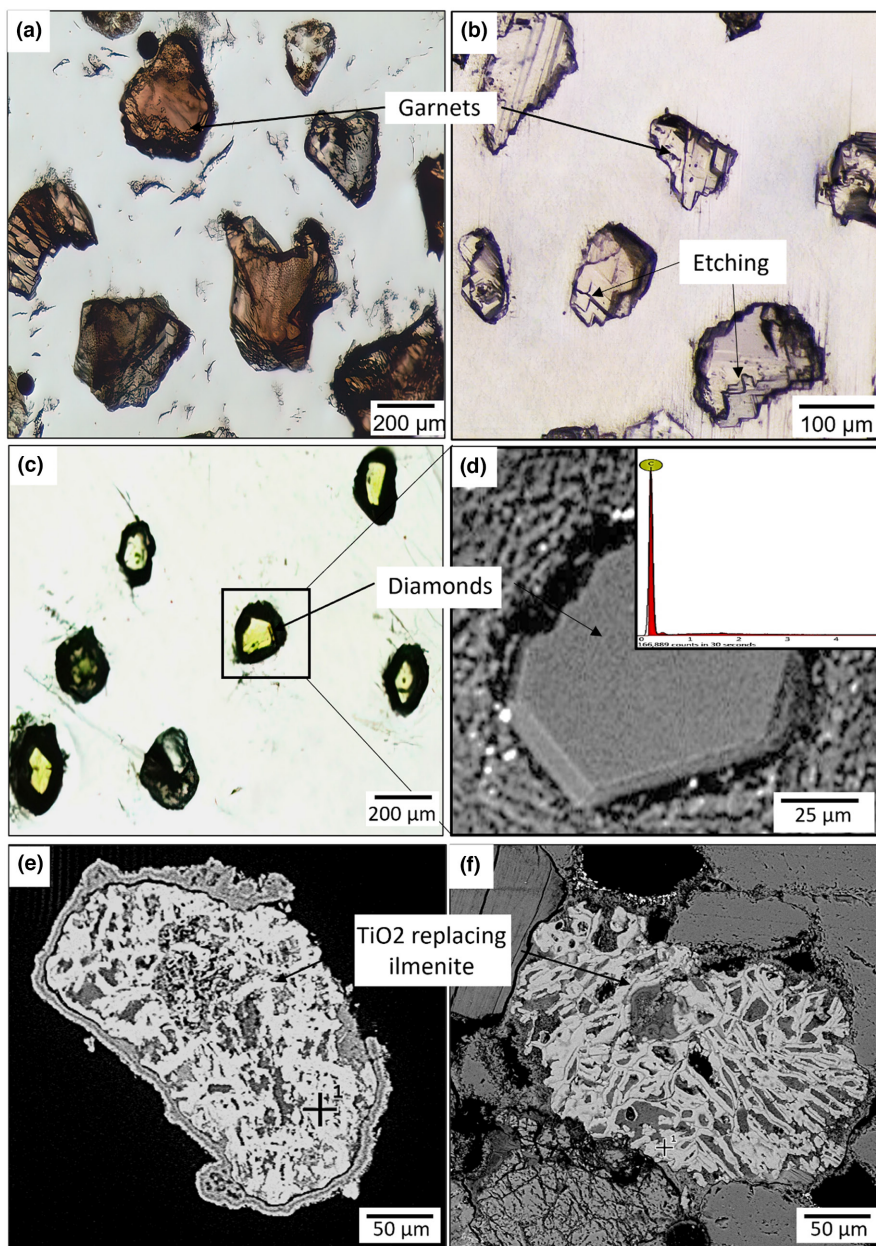


FIGURE 9 (a, b) Petrographic photomicrograph of garnet grains in the Duva field and the Agat field, respectively. Note the difference in the size and colour and the presence of etching patterns on those in the Agat field. (c) Petrographic photomicrograph of green diamond crystals observed at the limit between the UR and the LR showing (d) octahedron shape under SEM. (e, f) TiO₂ oxides (anatase or rutile) replacing ilmenite grains in the Duva field and the Agat field (Agat 100 mainly), respectively.

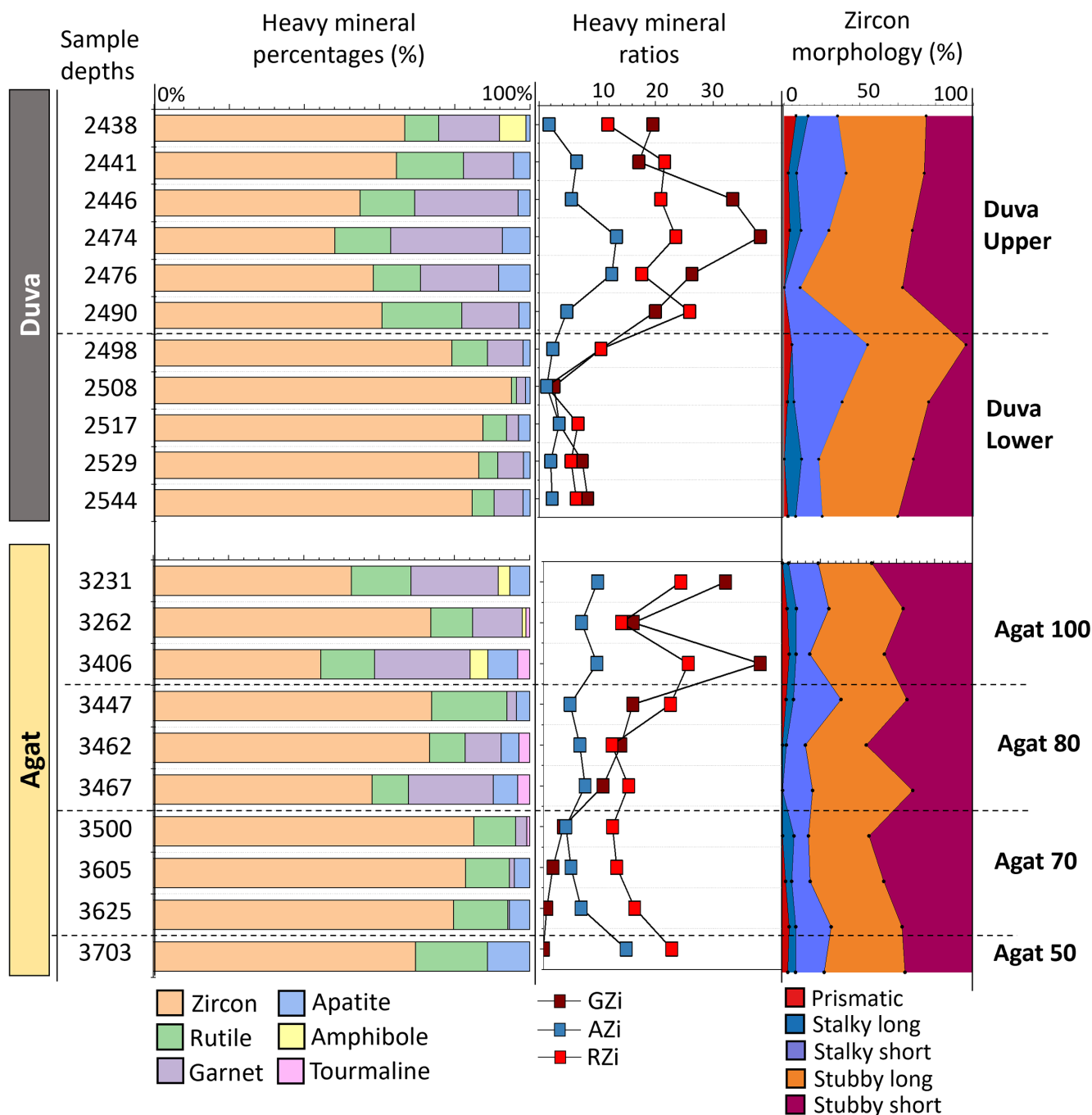


FIGURE 10 An overview of the heavy mineral percentages, computed indexes and zircon morphological groups of sandstones from the Agat and Duva fields.

One notable difference between the two reservoirs is also related to the size and morphology of garnets. In the UR, garnet is generally well preserved and is composed of coarse reddish grains with a size bigger than 350 μm and smaller uncoloured ones (<300 μm) (Figure 9a). In the LR, garnets are less common and are smaller in size showing etching patterns and alteration features. Traces of green diamond crystals were observed at the boundary between the UR and the LR (Figure 9c,d). The size of these diamonds ranges from 100 μm up to 170 μm.

In the Agat field, zircon also dominates the HM assemblage ranging from 44% to 85%. Zircon is highly concentrated in the Agat 70 and 50 compared to other units. The GZi shows an overall increase through the Agat 100, while RuZi and AZi seem to show less variation between the different Agat field units. Garnet is uncommon in the deepest samples (Agat 50) and is altered in the rest of the samples. Tourmaline and amphibole (tremolite and actinolite) are noted in many samples but mainly in small amounts (<4%).

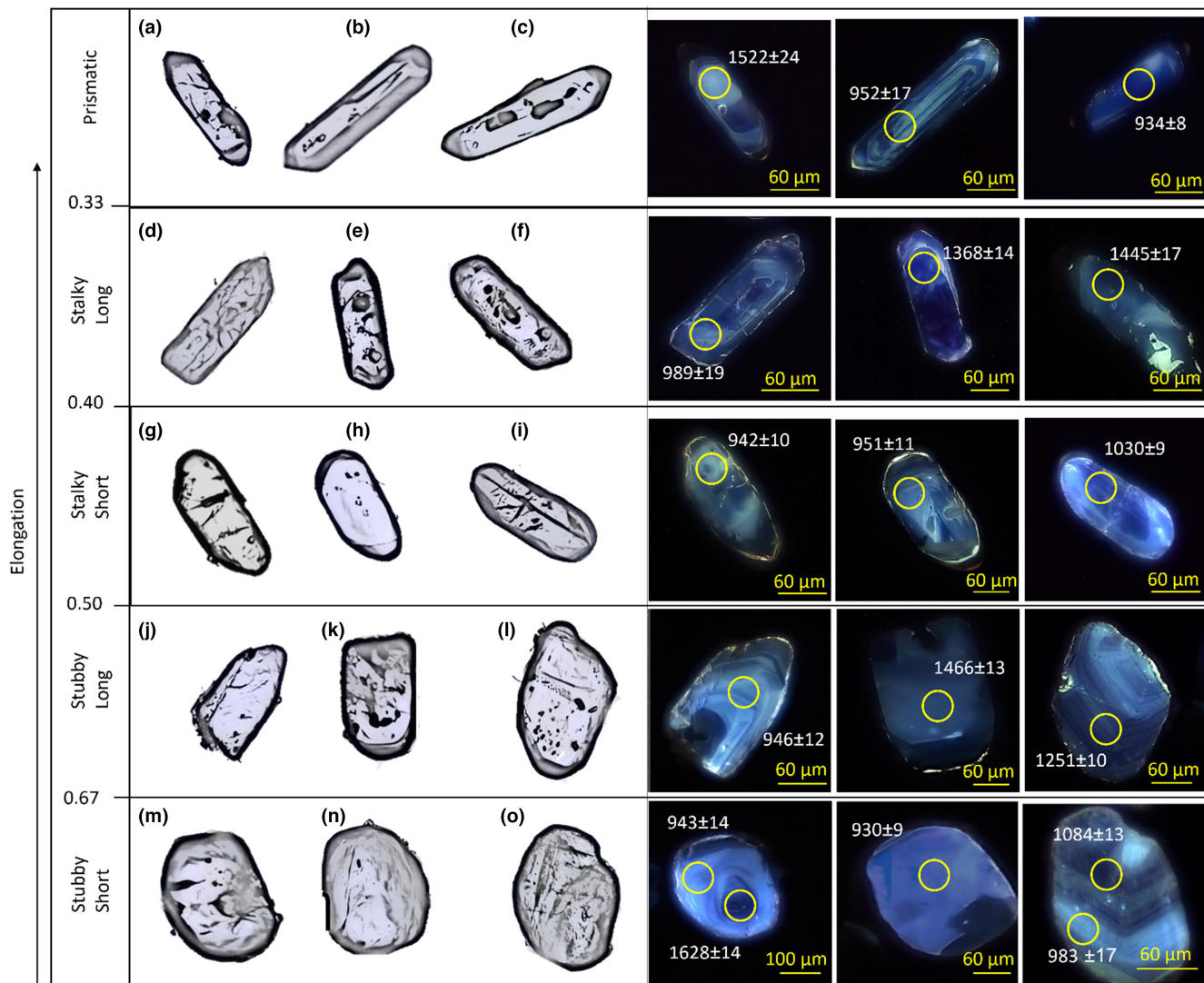


FIGURE 11 Illustrations of various groups of zircon morphologies observed in the Agat Fm. On the left are petrographic photomicrograph images and on the right are the corresponding cathodoluminescence images. (a–c) Prismatic zircons, (d–f) stalky long zircons, (g–i) stalky short zircons, (j–l) stubby long zircons, (m–o) stubby short zircons.

4.4 | Zircon characterisation

Elongation (El), defined as the ratio of width to length (Gärtner et al., 2013), is a morphological parameter to evaluate the transport and recycling history of zircons. Based on El, zircon in the Agat Fm can be classified into five main groups (Figure 11): (1) prismatic ($El < 0.33$), (2) stalky long ($0.33 < El < 0.4$), (3) stalky short ($0.4 < El < 0.5$), (4) stubby long ($0.5 < El < 0.67$), and (5) stubby short ($El > 0.67$). The abundance of these groups in the Agat Fm is shown in Figure 10. Overall, both the Agat field and the Duva field are dominated by stubby zircons, subordinate stalky zircons and rare prismatic zircons. However, zircon in the Agat field is dominated by well-rounded stubby short zircon, while the Duva field is dominated by stubby long zircons. Such a difference can be seen in Figure 12a. The Duva field shows unimodal distribution with a strong mode at 0.55

corresponding to stubby long zircons, while the Agat field shows polymodal distribution with modes at 0.54, 0.66 and 0.9. The presence of collision marks at the grain boundaries on many of the analysed zircon (Figure 11d,j,k,l) results from collision during transportation (Gärtner et al., 2013).

Cathodoluminescence (CL) imaging of zircons in the Agat Duva field (Figure 11) reveals metamorphic features. Most of the grains show a very complex internal texture, which is characterised by a weak CL emission and are either completely uniform (Figure 11k,n) or have very chaotic/distorted textures (Figure 11e,f,h,j). In some zircons, we distinguish dark CL cores that are surrounded by high-luminescent rims displaying sector zoning patterns (Figure 11j,i,m), corresponding to overgrowths (Figure 11j,m,o). Only a few grains display the typical habit of igneous zircon (Figure 11b,d), which are mainly prismatic and stalky.

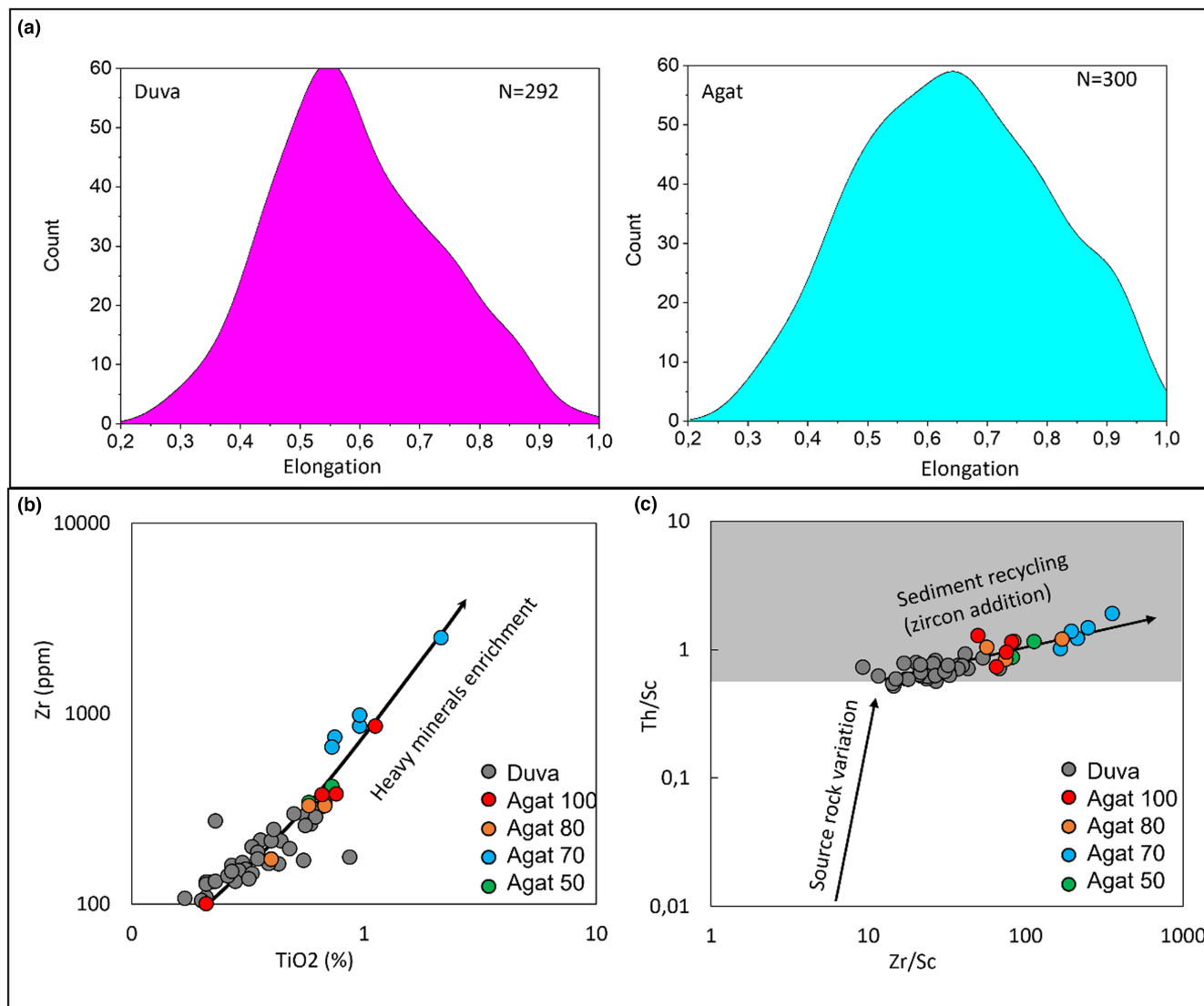


FIGURE 12 (a) Comparison of zircon elongation distribution between the Duva and Agat fields; (b) cross-plot of Zr vs. TiO₂ showing an overall increase in the Agat field typically in Agat 70; (c) Th/Sc versus Zr/Sc plot showing that the samples deviate from the compositional trend, implying the addition of zircon and suggesting a recycling effect.

Figure 12b shows the evolution of Zr concentration against TiO₂. A high enrichment of Zr and TiO₂ is noted in the Agat field, particularly in the Agat 70, where Zr reaches up to 2700 ppm and TiO₂ reaches up to 1.8%. This enrichment is associated with the high abundance of zircon and rutile observed in the Agat 70. Such enrichment could indicate sedimentary sorting and recycling. The Th/Sc versus Zr/Sc plot is widely used to assess the effects of sedimentary recycling and sorting (Chen et al., 2014; McLennan, 1989; Wang et al., 2019). Basic igneous rocks generally contain high Sc content, while felsic rocks are rich in Th. Therefore, fluctuation in Th/Sc ratios can reflect changes in source composition. However, the Zr/Sc ratio does not vary significantly with changes in source composition but is more sensitive to the process of sedimentary

recycling. Both the Duva and the Agat field follow a recycling trend with an important recycling effect recorded in the Agat field, particularly in the Agat 70.

4.5 | Zircon U–Pb geochronology

The results of LA-ICP-MS analyses, including ²⁰⁷Pb/²³⁵U ratios, ²⁰⁶Pb/²³⁸U ratios, ²⁷⁰Pb/²⁰⁶U ratios, and calculated ages, with the exclusion of discordant grains (<10% discordance), can be found in the supplementary materials. The obtained zircon age distributions are represented in Figure 13 showing the distribution of zircon ages in the different reservoir units along with kernel density estimate (KDE) plots.

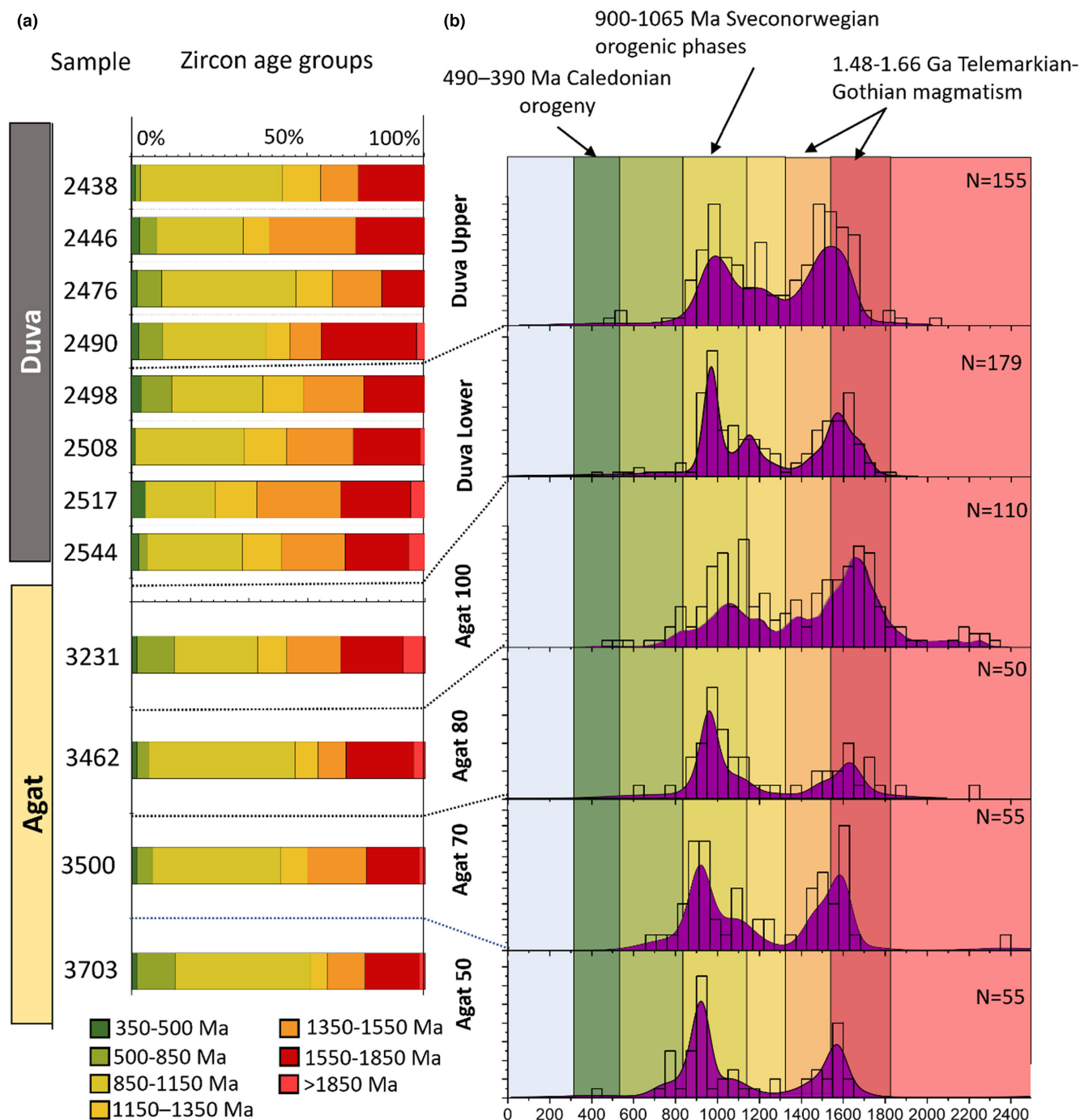


FIGURE 13 (a) Stacked bar chart showing the percentage of the different zircon age groups; (b) Histograms showing zircon ages for the different sandstone populations in the Agat Fm along with kernel density estimate age distribution curves (bandwidth: 50 Ma). *N* is the number of considered zircon U-Pb measurements (<10% discordance).

Three main groups of zircon ages are identified: 850–1150 Ma, 1350–1550 Ma and 1550–1800 Ma, with very few zircons older than 1800 Ma. These groups correspond to the major geodynamic events in Norway, including, from the youngest to the oldest, the Sveconorwegian orogenic phase, the Telemarkian orogeny, and the Gothian orogenic phase. Additionally, minor groups of ages are identified, including 350–550 Ma, 550–850 Ma and 1150–1350 Ma.

The relative abundance of these groups is represented in the form of stacked bar charts for each of the reservoir units (Figure 13a). Overall, the Duva field is dominated by 850–1150 Ma zircons, with a relative abundance ranging from 23.8% up to 48.3% (av. 35.3%) and by 1350–1550 Ma and 1550–1800 Ma zircons, which are equally present with an average of 20.4% and 22.7% respectively. The relative abundance of minor zircon ages, including those

between 350–550 Ma, 550–850 Ma and 1150–1350 Ma and >1800 Ma is 2.9%, 0.90%, 14.0% and 3.8%, respectively. The zircon age signatures of the UR and the LR are very similar, with a comparable proportion of 850–1150 Ma zircons (35.9% and 31.1%, respectively) and 1350–1850 Ma zircons (41.5% and 46.5%).

The zircon age signature in the Agat field is only slightly different from the Duva field in terms of the proportion of the main group ages showing a relative abundance of 42.0%, 15.2%, and 20.2% for 850–1150 Ma, 1350–1550 Ma, and 1550–1800 Ma, respectively. Also, a more significant proportion of 550–850 Ma zircons (av. 8.7%) is noted, together with a lower proportion of 1150–1350 Ma (av. 8.0%). Agat 50, 70, and 80 show similar zircon age distributions, which is significantly different from the Agat 100 showing a decrease in the proportion of 850–1150 Ma zircons (23%). Additionally, the proportion of older zircons >1800 Ma increases significantly in Agat 100.

Overall, the Duva field is dominated by 850–1150 Ma and 1350–1850 Ma zircons, which are distributed in equal proportion, while the Agat field shows a significant increase in the proportion of 850–1150 Ma zircons. However, the Agat 100 shares a closer distribution to the Duva field.

4.6 | Garnet composition

Garnet composition from the Duva and Agat field is illustrated in ternary diagrams in Figure 14, alongside garnet geochemistry in modern river sediments from Norway (Morton et al., 2004). The ternary diagrams show the variations of the garnet assemblages, which were quantified by determining the relative abundances of types A, Bi, Bii, Ci, and Cii (as defined by Morton et al., 2004). Type A garnets, have high Mg and low Ca, and are mostly found in high-grade metasedimentary rocks, charnockites, or

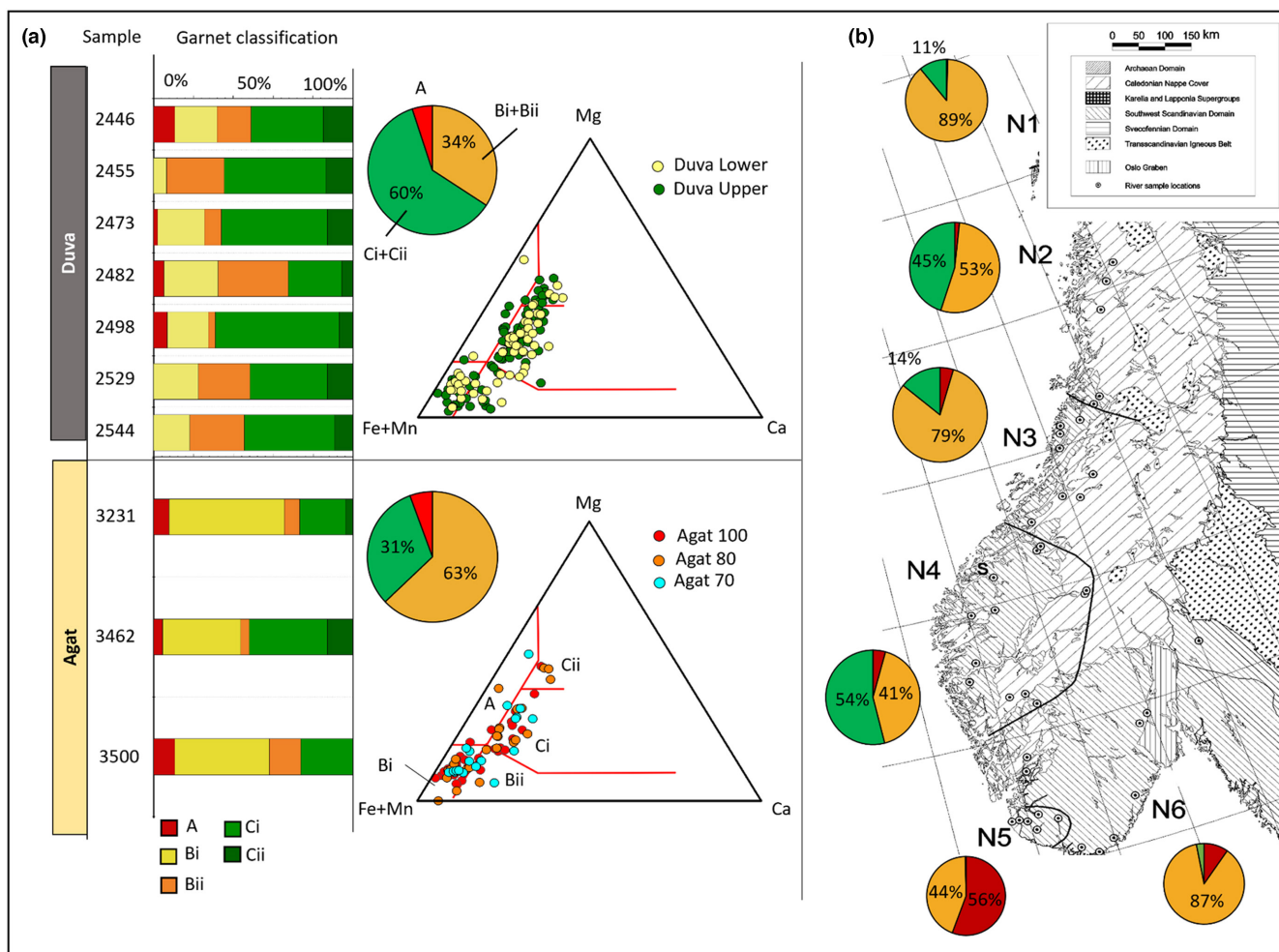


FIGURE 14 (a) Stacked bar chart and garnet geochemistry ternary plots showing the variations in abundance of garnet types for the Agat and Duva field (ternary plot classifications are based on Morton et al. (2004)); (b) Figure: Garnet geochemistry variation in river sediments from different regions in Norway, indicating a higher concentration of type C garnets in the N4 area compared to other regions (adapted from Morton et al. (2004)).

intermediate-silicic deep crustal igneous rocks. Type B has low Mg and variable Ca, is commonly rich in Mn, and can have various sources such as lower amphibolite facies, metasedimentary rocks, and intermediate-acidic meta igneous rocks. Type B is generally divided into two subgroups: Bi extremely rich in Fe mainly corresponding to granitoids and pegmatites and Bii with higher Ca mainly corresponding to low-medium grade metasedimentary rocks. Type C has high Mg and high Ca and is generally found in high-grade mafic and ultramafic gneisses, and is subdivided into subgroups: Ci and Cii, which separate garnets from meta-mafic rocks and meta-ultramafic rocks respectively.

The proportion of the various garnet types is shown in Figure 14a for the different reservoir units. Garnet geochemistry shows a significant variation between the Agat and the Duva fields, primarily in terms of the percentage of type B and type C garnet. In the Duva field, the garnet populations are mostly dominated by type Ci garnet with a relative proportion ranging from 36.1% up to 62.0% (av. 45.5%). Ultramafic type Cii garnet shows a relative proportion of 9% on average, while Bi and Bii show a relative proportion of 19.9% and 20.8%, respectively. Type A is uncommon, with a proportion of less than 4%. Both the UR and the LR in the Duva field show similar garnet geochemistry on average with only a slight increase in type Ci and Cii observed in the lower reservoir.

In the Agat field, garnets are dominated by type Bi, which ranges in proportion from 39.1% up to 57.6% (av. 48.0%) while Bii ranges from 4.3% up to 15.7% (av. 9.2%). The average proportion of type Ci and Cii garnets is 29.5% and 5.6% respectively. However, the Agat 80 has a higher proportion of type Ci (av. 39.1%) and Cii (av. 13.0%) garnets compared to the other Agat units. Additionally, garnets type A are more common in the Agat field showing an average proportion of 7.5%.

Overall, garnet in the Duva field is composed of two main origins: a type C garnet reflecting a high-grade mafic source associated with subordinate type B garnet reflecting a felsic source associated with lower-grade metamorphic rocks. Conversely, the Agat field is dominated by type Bi reflecting a strong contribution from felsic low-grade metamorphic rocks with subordinate type C garnet reflecting a weaker contribution from high-grade metamafic rocks.

5 | DISCUSSION

5.1 | Diagenetic control on mineralogy and chemistry of the sandstone

Diagenetic evolution in the Agat Fm was widely explored by Azzam et al. (2022, 2023), Hansen et al. (2021), and Patrier et al. (2023). These studies show that the pristine

mineralogical composition of the Agat Fm was greatly modified through the authigenesis of clay minerals (mainly chlorite and kaolinite), dissolution of unstable minerals such as feldspar, and cementation of carbonates (siderite and calcite). Although the diagenetic reactions in the Agat and Duva fields were comparable, the intensity of these reactions varied significantly. This variability can be attributed to two key factors: (1) the amount of Fe originally present in the sediments and (2) the degree of openness of the diagenetic system, which determines the fate of dissolved by-products.

Chlorite is the main authigenic mineral in the Duva field, representing up to 25% of the total rock volume in the Lower Reservoir (LR), but less than 7% in the Upper Reservoir (UR). In contrast, chlorite abundance in the Agat field ranges from 2% to 12%. In the Duva field, chlorite has a high iron content ($X_{Fe} > 0.88$), primarily due to the original composition of the sandstone, which includes a high concentration of glauconite, Fe-illite, and Fe-ooids/peloids (Azzam et al., 2022, 2023). In the Agat field, however, chlorite is richer in magnesium (X_{Fe} ca. 0.71–0.75), mainly due to the dissolution of biotite and Fe-bearing clays such as HIMs and detrital kaolinite (Azzam et al., 2023). Polytype Ib ($\beta = 90^\circ$) is dominant in both the Agat field and the Duva field, supporting a transformation from a berthierine precursor (Azzam et al., 2023; Beaufort et al., 2015; Patrier et al., 2023). Based on XRD analysis, the studied samples do not contain any traces of corrensite, thereby excluding a transformation from tri-octahedral smectite (saponite). If corrensite was completely transformed into chlorite at the present burial temperature (105–129°C), then polytype IIb should be dominant (Azzam et al., 2023; Beaufort et al., 2015; Patrier et al., 2023). However, polytype IIb is a minor component in the samples studied, indicating that only minor amounts of Fe-chlorite may have been derived from corrensite or more likely have a detrital origin. The formation pathway of chlorite in the Agat Formation can be summarised as follows:

1. Berthierine formation commenced with the dissolution of detrital clay minerals, likely pedogenetic kaolinite and hydroxy-interlayered clays derived from weathered soil profiles on the Norwegian mainland during the Lower Cretaceous (Lidmar-Bergström et al., 1997).
2. Under reducing early diagenetic conditions facilitated by microbial activity, Fe^{2+} was released from the alteration of Fe-bearing detrital grains and clays, leading to the nucleation and growth of berthierine (Azzam et al., 2022; Murakami et al., 2004; Sugimori et al., 2009; Virolle et al., 2022). Low sulphate prevented pyrite formation, favouring berthierine precipitation (Azzam et al., 2022).

3. With increasing burial temperatures exceeding 50°C, the metastable berthierine underwent a solid-state transformation to chlorite (Beaufort et al., 2015; Virolle et al., 2022). This transformation is nearly complete at the current reservoir temperatures of 80–129°C.

In the Agat field, there is a correlation between secondary porosity from feldspar dissolution and kaolinite presence. Feldspar dissolution provided aluminium for kaolinite to precipitate, but it occurred mainly during late diagenesis since early diagenesis shows preserved feldspar grains and minimal kaolinite. Feldspar dissolution is primarily driven by acidic pore waters, which are mainly generated from organic acids during the maturation of organic matter (Schmidt & McDonald, 1979; Surdam et al., 1989; Yuan et al., 2015). Dissolved feldspar by-products are redistributed throughout the pore system and precipitate as secondary minerals such as kaolinite, and locally as quartz overgrowth. This process typically occurs in a closed diagenetic system (Xiao et al., 2018), which contrasts with the Duva field, where an open diagenetic system is implied due to the lack of secondary kaolinite precipitation (Azzam et al., 2022).

Carbonate cementation, such as siderite and calcite, primarily affects the CaO and LOI values. When carbonates are scarce, the variations in LOI are mainly due to the dehydration of clay minerals. This explains the two trends shown in Figure 7, which reflects the distribution of carbonates and clay minerals. The presence of calcite cement is also responsible for the positive Sr anomaly found in the Agat field and some samples in the Duva field.

The Duva field also contains common diagenetic apatites that derive from the leaching of phosphatic concretions. These diagenetic apatites are responsible for the high P₂O₅ content found in the Duva field.

5.2 | Reconstructing the sediment routing system

5.2.1 | Depositional environment: Role of inherited topography

The most distinguished parameter between the Agat field and the Duva field is the texture and the sorting of the sandstone. The strong difference in textural characteristics between the two turbidite systems reflects significant changes in the transport-depositional characteristics during the Lower Cretaceous. Based on the classification of Bouma (2000), the Duva field exhibits all the characteristics of a coarse-grained turbidite system showing a high sand/shale ratio, low vertical shale interbeds with sediments that are poorly sorted, and gradually outbuilding

into the basin. Conversely, the Agat field displays typical characteristics of a fine-grained turbidite system characterised by overall well-sorted grains with a relatively moderate sand/shale ratio.

Coarse-grained turbidite systems are common in active margins (Bouma, 2000). They are distinguished by a short distance between the sediment source and the coast, narrow shelves, and a steep gradient of the fluvial system. The fan system is built through progradation, resulting in a high sand/shale ratio. On the contrary, fine-grained turbidite systems are typical of passive margins (Bouma, 2000). Their source of sediment is located far from the coast with a low gradient of the fluvial system. The shelves are wide with gentle slopes. The deltaic system is often large, and the fan system is constructed through a bypass, fed by major fluvial-deltaic systems that require a significant sea-level drop to reach the shelf break (Bouma, 2004). Most of the turbidite systems in the Northern North Sea basin during the Cretaceous and the Paleogene (e.g. Kyrre Fm, Nise Fm, Springar Fm, Heimdal Fm, Tang Fm) are fine to medium-grained, with only a few instances of coarse-grained sandstone (e.g. Hauterivian sandstones in Slørebotn sub-basin) (Lien et al., 2006; Martinsen et al., 2005). The presence of coarse clastic sediments in the Slørebotn sub-basin is related to the presence of high reliefs along the scarp of faults inherited from Jurassic rifting. Sediments were mainly deposited in small and narrow sub-basins fed from small drainage areas located close to the depositional zone (Martinsen et al., 2005). The Frøya High (North of Slørebotn sub-basin) features several incised canyons at its crest that cut deeply into the basement acting as pathways for the transport of coarse clastic sediments (Bukta, 2018). These canyons were established during the late Jurassic following rifting and deepened during the Lower Cretaceous (Bauck et al., 2021). These deeply incised canyons are very similar to those observed in the Duva field based on seismic data (Neptune Energy internal report). The depositional model of the Hauterivian sandstone was likely similar to the Duva turbidite system formed at steep slopes in small and narrow sub-basins. Sediments were transported in structurally confined canyons as confirmed by 3D seismic data. The drainage area was probably small and close to the zone of deposition as suggested by the immature composition of the sediments. The Agat system, on the other hand, shows less confinement based on 3D seismic data (VNG, internal report). The channels are weakly amalgamated with more lateral migration suggesting a larger depositional area and a gentler slope. The sediments are likely fed from a larger source area as suggested by the size of the turbidite system which is three times bigger than the Duva turbidite system.

In summary, the texture of turbidite systems during the Lower Cretaceous was largely controlled by inherited

bathymetry from the Jurassic rifting. Coarse-grained turbidite systems (e.g. Duva turbidite system) were more restricted to small confined sub-basins formed at the edge of steep slopes that are close to the sediment source.

5.2.2 | Sediment provenance

5.2.2.1 | Duva turbidite system

Sandstones of the Duva field are typically litharenite to feldspathic litharenite containing a high proportion of metamorphic rock fragments, as well as many quartz grains displaying undulose extinction, testifying of a strong contribution from a metamorphic source (Basu et al., 1975). Feldspar is mainly composed of orthoclase, microcline and perthitic feldspar with scarce plagioclase suggesting a felsic source. Also, a small component of volcanic rock fragments is detected suggesting the presence of some volcanic terranes in the drainage area.

Both the LR and the UR in the Duva field are similar in terms of mineralogical composition but show significant quantitative variation in terms of chemistry and mineralogy. Fe grains are strongly concentrated in the LR, while there is an increase in the amount of quartz and feldspar in the UR. Azzam et al. (2022) and Patrier et al. (2023) attributed the quantitative changes between the two reservoirs to be the result of progressive erosion and denudation of saprolite profiles developing on the protolith. During the deposition of the LR, the sediments were supplied from saprolite profiles, which form the main source of Fe and fine fraction materials. During the deposition of the UR, the sediments are progressively supplied from weakly altered rocks or the parent rocks.

Heavy mineral quantification reveals the abundance of zircon in the LR and the substantial increase of garnet, apatite, and rutile in the UR. The high concentration of zircon in the LR suggests an ultra-stable composition, which can be attributed to the intense chemical weathering of the less stable minerals in saprolite profiles, probably in acidic soil settings (Morton & Hallsworth, 1999). Conversely, the increase of garnet, apatite, and rutile in the UR suggests an increasing input from the protolith when saprolite profiles were denuded. Additionally, the strong increase in garnet size in the UR indicates a direct contribution from the metamorphic source. In addition, the presence of some diamond crystals detected at the limit between the UR and the LR suggests the erosion of ultra-high metamorphic rocks in the drainage area.

Garnet chemistry from the Norwegian landmass shows that area N4, located east of the study area, supplies garnet populations similar to those found in the Duva field (Figure 14b) (Morton et al., 2004). Morton et al. (2004) indicated that Mg content in garnets varies significantly

depending on the composition of the metamorphic rocks: High-Mg garnets are typically found in ultramafic rocks, moderate Mg garnets are typically found in mafic rocks, and low-Mg garnets correspond to intermediate-acidic rocks and granites/pegmatites. The western gneiss region consists mainly of Precambrian gneissic rocks, which also contain high-grade basic gneisses (including eclogites). and locally, pyroxenites and peridotites are present (Cuthbert et al., 2000; Ravna et al., 2006). Based on the chemistry of garnets in the Duva field, the sediments are dually sourced from (1) a metamorphic source consisting of meta-mafic rocks (including eclogites) and subordinate meta-ultramafics (such as peridotites and pyroxenites), (2) a felsic source, associated with lower-grade metamorphic rocks (e.g. quartzo-feldspathic gneisses) with some high-Mn garnets (subfield Bi) possibly sourced from granitoid rocks. In addition, many localities in the western gneiss, like the Nordøyane UHP domain, host eclogite/coesite and micro diamond-bearing rocks (Butler et al., 2013; Cuthbert et al., 2000), which could be a potential analogue to the high-grade metamorphic source in the Duva field. No significant differences were found in the chemical composition of garnets between the LR and UR, supporting similar sources for the two reservoirs.

Most zircons in the Duva field are metamorphic with small proportions of igneous zircons. Zircons are mostly rounded and stalky, suggesting that they have been recycled. The detrital zircon ages in the Duva field match those found in the western gneiss region (Figure 15) (Bingen & Solli, 2009). The basement rocks of the western gneiss contain widely spread 1749–1650 Ma and 1649–1520 Ma zircons that match the detrital 1550–1800 Ma zircons group in the Duva field. It also contains 1519–1470 Ma, 1469–1400 Ma, and 1399–1200 Ma zircons corresponding to the detrital 1350–1550 Ma and 1150–1350 Ma zircon groups identified in the Duva field. The area also has an abundance of 999–850 Ma zircons, which match the younger detrital 850–1150 Ma group. These groups of zircons record major magmatic episodes that correspond to the Gothian—Telemarkian (1.52–1.66 Ga and 1.48–1.52 Ga, respectively) and Sveconorwegian (0.92–1.04 Ga) orogenic periods (Wiest et al., 2018). There is also a small component of 350–550 Ma zircons that likely correspond to the Caledonian orogeny (Scandian phase) (Fossen et al., 2017).

In summary, the provenance of Duva sandstones can be mostly tied back to the Western Gneiss Region. This region underwent intense metamorphism during Precambrian and Palaeozoic times. The source of sediments can be compared to the actual UHP domains that are found on the Eastern margin of the Western Gneiss Region. These domains contain mixed mafic (mainly eclogite) and felsic (granite and quartz feldspathic gneisses) rocks, which

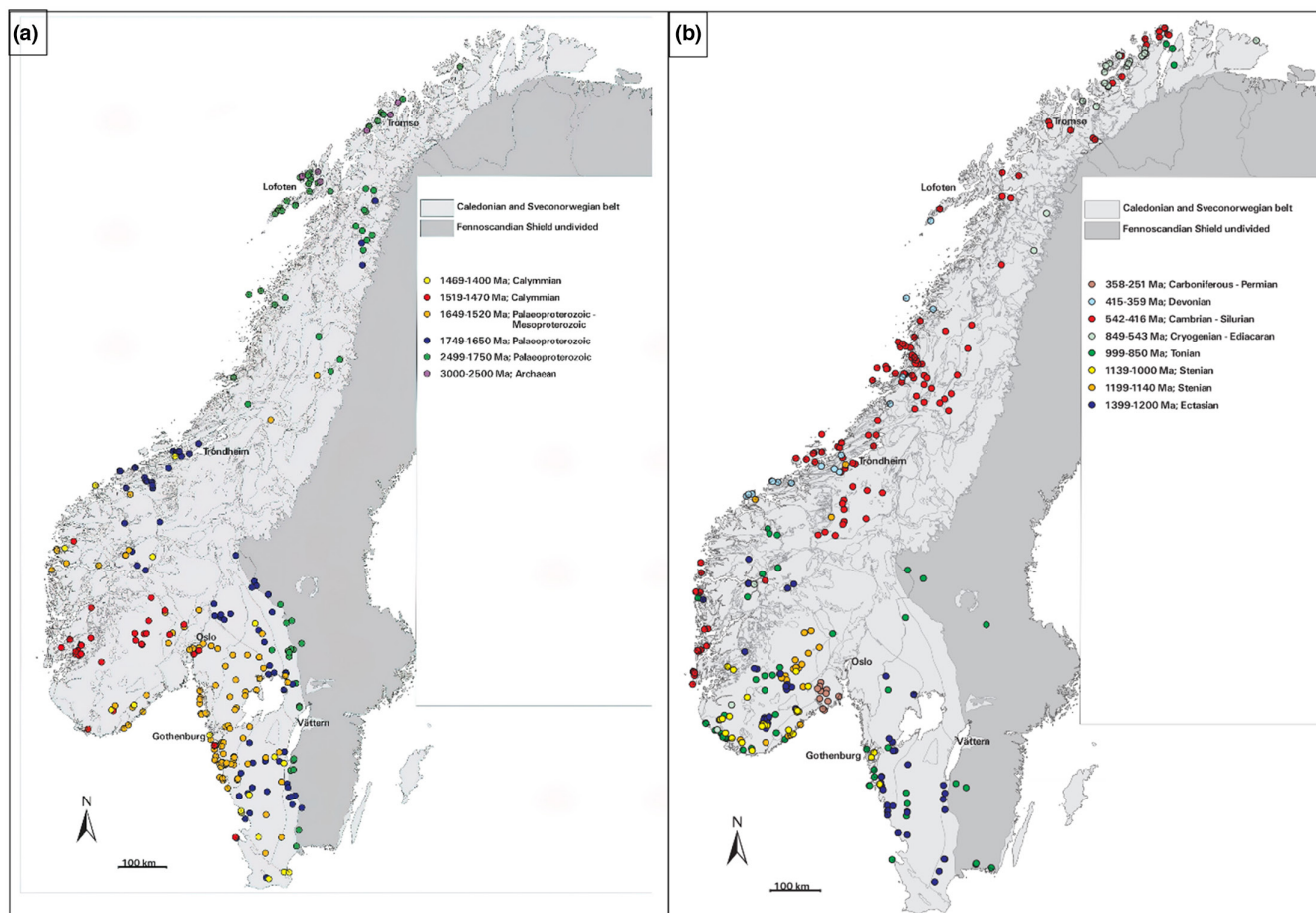


FIGURE 15 Summary of zircon ages distribution in Scandinavia, compiled by Bingen and Solli (2009). Map of zircon age distribution: (a) Ages between 3000 and 1400 Ma, (b) ages between 1400 Ma and 251 Ma.

are reflected by the chemistry of garnets in the Duva field. Finally, combined petrographic observations and heavy minerals data suggest similar sources for the LR and UR. The difference between the mineralogy of the two reservoirs is explained by weathering/denudation processes.

5.2.2.2 | Agat turbidite system

Sandstones in the Agat field are typically subarkosic dominated by monocrystalline quartz and subordinate polycrystalline quartz with a small proportion of metamorphic lithic fragments. Agat 100 however contains a higher proportion of metamorphic fragments than the other units. Additionally, the Agat field contains a significant amount of K-feldspar and plagioclase compared to the Duva field. These observations confirm the weaker contribution from metamorphic sources. The relative increase of plagioclase in the Agat field could either be explained by chemical weathering processes or related to the source composition. Since plagioclase is less stable than K-feldspars and tends to dissolve faster in regoliths (White et al., 2001), its presence could indicate low chemical weathering rates or high denudation rates of the protoliths. An increase in

plagioclase content could also indicate a more basic composition of the source rocks (Clark, 1966).

Heavy minerals in the Agat field are quite similar to those in the Duva field in terms of the species identified. However, tourmaline and amphibole are more common in the Agat field. The GZi index varies significantly between the different units, while AZi and RZi are more stable. Extremely low GZi is observed in Agat 70 and Agat 50, which is related to the high concentration of zircon in these units. This is attested by Zr content in Agat 70 reaching 2500 ppm. Rutile seems to follow the same trend as zircon showing a significant increase in Agat 70 and Agat 50. Zircon and rutile are both resistant to physical transport conditions, so they tend to concentrate on sediments with increasing sorting. Previous palaeogeography reconstruction of Agat 70, 80, and 100 by VNG Norge suggests that Agat 70 and probably Agat 50 are supplied from different sediment entry points. The Agat 70 sandstones probably experienced a higher degree of reworking and sorting on the shelf before their deposition in deep marine settings. As shown in figure (Figure 12c) the recycling/sorting effect is far more superior in the Agat field compared to the

Duva field. This is consistent with the texture of the sandstone, which suggests longer transportation distances and better sorting.

Garnet in the Agat field shows common etching features, which indicate some influence of deep burial diagenesis (Morton & Hallsworth, 1999). Our petrographic observations show that garnets are still preserved below 3600 m despite the common etching feature suggesting that it can be still used as a provenance indicator (Morton et al., 2004). The garnet signature in the Agat field is very different from the Duva field. Type B garnets are dominant in the Agat field with subordinate type C suggesting input from low-grade metamorphic or granitoid rocks with weaker input from meta-mafic rocks (eclogites). Another key difference is also the higher proportion of subtype Bi compared to Bii subtype, which suggests that the felsic component is largely composed of granitoids. This is also supported by the presence of tourmaline in that field, which is commonly attributed to granite and pegmatite rocks (Kotowski et al., 2020). The garnet signature in the Agat field does not correspond directly to Area N4 but rather seems to represent a mixture between Area N3 and N4 (Figure 14b). Area N3 in northern west Norway features complex lithologies composed of upper allochthon metasediments and has wide exposures of gneisses, granites, and gabbros (Morton et al., 2004). There are few eclogite exposures in this area, but they are far less important than those found in area N4 in the Western Gneiss Region.

Zircons in the Agat field show metamorphic features, with only a small proportion retaining igneous characters. However, zircons in the Agat field exhibit a more rounded morphology, particularly in the form of stubby zircons, indicating a higher degree of transportation and sorting. There are certain similarities in the zircon age signature between the Duva and Agat fields, with some differences in the proportion of the main zircon age groups. For instance, the Agat field contains a significantly higher proportion of 850–1150 Ma zircons, except for the Agat 100, which has a proportion similar to the Duva field.

5.2.3 | Climates and chemical weathering

Tracing the paleoclimate conditions can be a challenging task owing to the great diversity of processes that can affect the original mineralogical composition of sediments before or after their deposition. Many proxies have been proposed in the literature to evaluate the intensity of chemical weathering and alteration. Clay minerals in sediments, especially marine sediments, are useful indicators of paleoclimate (Brekke, 2000; Deepthy & Balakrishnan, 2005; Singer, 1984; Thiry, 2000). The intensity of chemical

weathering can also be evaluated using the chemical Index of Alteration (CIA), which is considered a widely accepted weathering index for reconstructing past climate conditions (Goldberg & Humayun, 2010; Heinrich & Nicole, 2011; Meunier et al., 2013). However, these proxies must be approached critically and factors such as the distinction between authigenic and detrital clay minerals, the relationship between climatic parameters and clay mineral formation, post-depositional diagenetic changes, and differentiation during transport, must be considered (Singer, 1984; Thiry, 2000). Diagenesis has greatly altered the original mineralogical assembly of the sediments in the Agat Fm. Most of the inherited detrital clay fraction in the Duva field has been transformed into authigenic chlorite (Figures 5d and 6) (Azzam et al., 2022). In the Agat field, the precipitation of authigenic kaolinite in addition to chlorite makes it difficult to fully decrypt the original detrital signature of the clays (Azzam et al., 2023). Additionally, the precipitation of carbonates and the dissolution of feldspar make it challenging to calculate the CIA index. In this study, we used two proxies to evaluate the intensity of chemical weathering: (1) by focusing on some minerals sensible to chemical alteration like Mica and by identifying the nature of detrital clays, (2) by studying trace element distributions. There is a significant difference in the composition and distribution of micas between the Agat field and the Duva field. While the former is dominated by biotite and muscovite and traces of glauconite, the latter is dominated by Fe-illite grains and glauconite with scarce biotite and muscovite. Fe-illite grains are important to evaluate chemical weathering since they typically form from pedogenetic alteration (Price & Velbel, 2014). For many years, these grains were considered typical glauconite or expanded mica grains (Ehrenberg, 1993) without any consideration of their origin. These grains show some morphological similarities to biotite, but they are highly expanded along the c-axis resembling kaolinite (Figures 5b,c and 16a). According to Patrier et al. (2023), this morphology of Fe-illite in the Agat Fm is inherited from the supergene vermiculitisation of large phyllosilicates in saprolite (mainly biotite). Alteration of biotite into vermiculite is witnessed in many Mesozoic Scandinavian saprolitic remnants (Fredin et al., 2017; Lidmar-Bergström et al., 1997, 2009; Olesen et al., 2012). Biotite weathering into vermiculite typically occurs under acidic leaching conditions in humid temperate/subtropical regions (Lidmar-Bergström et al., 1997; Loveland, 1984). These conditions prevailed during the Lower Cretaceous, allowing the development of deep saprolite or laterite profiles in some areas in Western Norway (Lidmar-Bergström et al., 1997). Based on these facts, the ratio of Fe-illite grains over primary micas minerals (biotite/muscovite) can be used as a paleo weathering

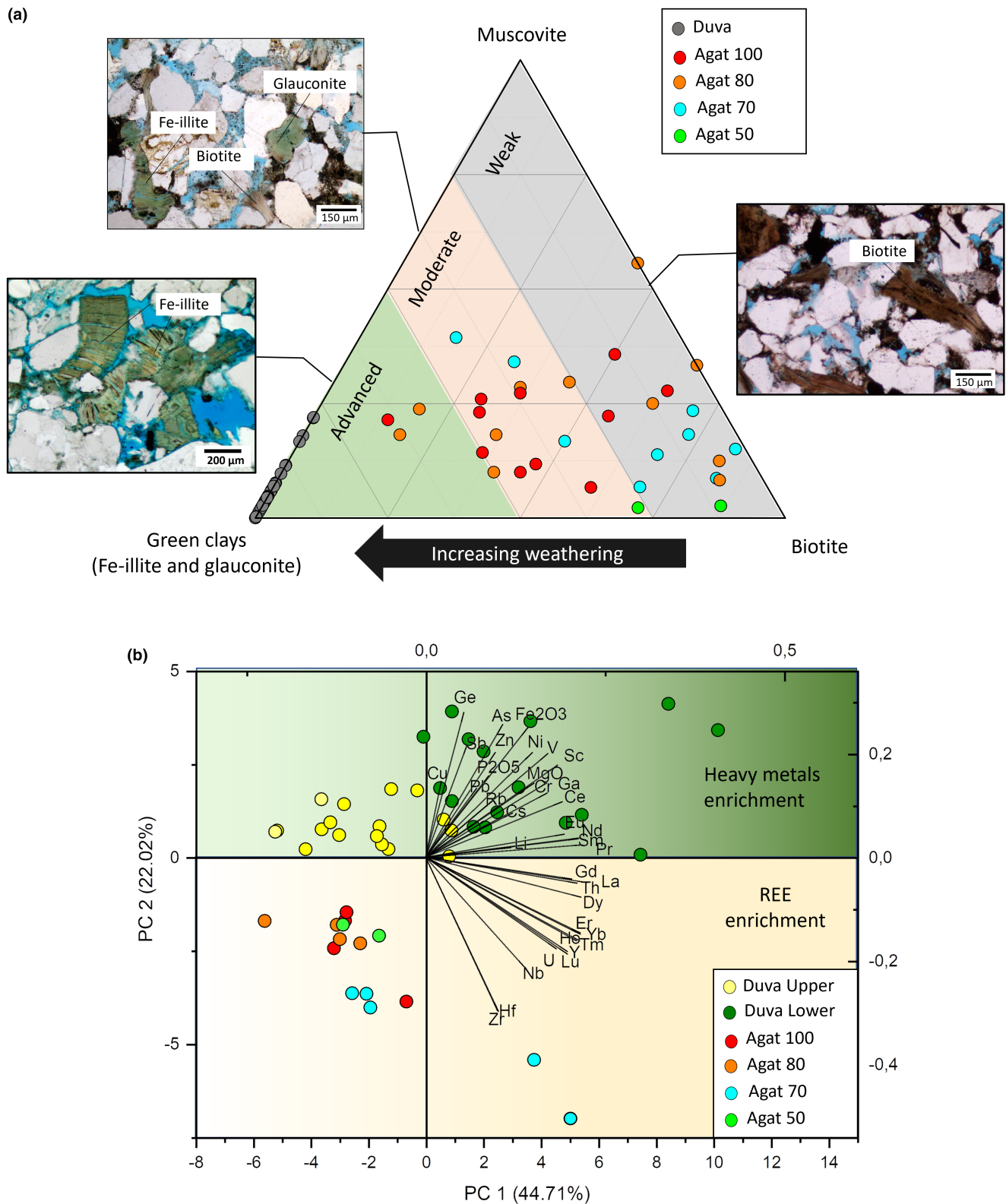


FIGURE 16 (a) Ternary plot of muscovite-green clays-biotite to evaluate the intensity of chemical weathering. The Duva field falls in the strong weathering domain, while most of the studied samples in the Agat field fall in the weak to moderate weathering domain containing fresh biotite and muscovite that are weakly altered; (b) principal component analysis (PCA) diagram of some selected trace metals and REEs, showing a strong variation in the Agat Fm related to the inherited source and paleoclimate conditions.

indicator with Fe-illite being the end-product of intensive chemical weathering. As shown in Figure 16a, the Duva field is mainly supplied from highly weathered bedrock in contrast to the Agat field. The presence of detrital kaolinite (iron bearing) in deformed ductile rock fragments indicates extensive development of laterites in the source area. Most of these detrital kaolinites are transformed into chlorite during burial diagenesis (Figure 5d). In the Agat field, the rare occurrence of Fe-illite and the preservation of primary micas (biotite/muscovite) indicate a weak supply from saprolites. Figure 16a shows that Agat 70 and 50 are supplied from weakly weathered bedrock, while Agat 80 and Agat 100 are supplied from more moderately weathered bedrock. This is consistent with the higher amount of residual pedogenetic clays in the Agat 80 and Agat 100 consisting of hydroxy-interlayered clays and illite (HIMs) mixed with kaolinite (Figure 5h) (Azzam et al., 2023). This also explains the high amount of plagioclase in Agat 50 and 70 compared to Agat 80 and Agat 100, which are primarily composed of K-feldspars. Another important proxy to evaluate the intensity of the chemical weathering is the distribution of trace metals (Ni, Cr, V, Sc, Zn, Ga, Li, Pb, Zr...) and REEs. A Principal Component Analysis (PCA) was conducted to analyse the distribution patterns of selected trace metals and REEs in both the Agat and Duva fields (Figure 16b). The first principal component (PC1) explains 44.7% of the data variability and distinguishes between Metal-REEs enriched sandstones and depleted ones. The second principal component (PC2) accounts for 22.0% of the data variability and separates heavy metals enrichment from REE enrichment. The Duva field is enriched in trace metals (V, Ni, Cr, Sc, Zn, Ge, Pb, As) and some REEs (Ce, Nd, Sm), which seem to correlate positively with Mg and Fe. The Agat field on the other hand is strongly depleted in trace metals but some samples are highly enriched in REEs, which is typically associated with zircons. This explains why certain samples in Agat 70 are highly enriched in Zr, Hf, U, and REEs. Trace metals such as Pb, Zn, Ni, Cr, Co and V are highly enriched in saprolites developing under a humid tropical environment (Ansart, 2022; Sharma & Rajamani, 2000; Taylor & Eggleton, 2001; Tijani et al., 2006). Strong enrichments of heavy metals and REE in some Norwegian tills were also interpreted to be the result of a deep weathering process under humid climate conditions (Olesen et al., 2012). In the saprolites, these elements are mainly hosted in the form of Fe-oxides-oxyhydroxides and clay minerals (e.g. kaolinite, smectite, illite) (Sharma & Rajamani, 2000; Tijani et al., 2006). These minerals can be eroded and transported into marine environments serving as precursors for chlorite, which can incorporate these trace metals into its structure. Therefore, the relatively high enrichment of trace metals in the LR of the Duva field

could reflect a strong input of materials from saprolites. Additionally, the strong positive Ce-anomaly detected in the Duva field is mainly attributed to the presence of cerianite (observed under SEM), a mineral that is typically found in lateritic profiles (Braun et al., 1990). The Agat field, on the other hand, shows strong depletion in trace metals indicating a very weak development of saprolites or alteration profiles.

The Agat Fm also comprises some altered minerals, which have a morphology that resembles ilmenite, mainly composed of TiO_2 with less than 2% Fe_2O_3 . These minerals are ubiquitous in the Duva field forming most of the opaque fraction of heavy mineral assemblages. They are also noted in Agat 80 and Agat 100. The alteration of ilmenite is generally attributed to leaching caused by supergene processes (Mücke & Bhadra Chaudhuri, 1991). The leaching of ilmenite is promoted in oxidising and acidic environments, which enable the formation of pseudorutile, which in turn can transform into leucoxene and to anatase/rutile as a final product (Anand & Gilkes, 1984; Cornu et al., 1999; Hugo & Cornell, 1991; Knudsen et al., 2015; Mücke & Bhadra Chaudhuri, 1991). Such a mechanism of leaching is pervasive in tropical environments such as in the Amazon basin, where ilmenite is strongly altered in hot humid climates while being preserved under dried conditions (Knudsen et al., 2015). The presence of altered ilmenite in the Agat Fm could further support a hot humid climate in the Duva field source area and probably the establishment of a more humid climate during the deposition of Agat 80 and 100 in the Agat field. However, the use of ilmenite alteration as a paleoclimate indicator must be approached carefully since ilmenite alteration was also reported during diagenesis under both oxidising and reducing conditions (Mücke & Bhadra Chaudhuri, 1991; Weibel & Friis, 2007).

In summary, the source rock was subjected to different degrees of chemical alteration, which has greatly influenced the mineralogy of the Agat Fm. The source of materials in the Duva field (typically the LR) was mostly associated with saprolite or laterite profiles formed under warm humid climates. The advanced chemical weathering promoted the alteration of biotite into vermicular Fe-illite grains and the enrichment in fine fraction materials hosting heavy metals (V, Ni, Zn, Cr...). Conversely, the Agat field was sourced from weakly to moderately altered bedrocks and the weathering profiles were probably very thin resulting in low concentrations of trace metals. Although both the Agat and Duva fields primarily originate from source rocks in western Norway, differences in tectonic uplift and geomorphic response are likely to have resulted in the outcrop of a heterogeneous hinterland geology on the Norwegian mainland. While some regions preserve

thick, well-developed alteration profiles due to tectonic stability and limited erosion, others lack distinct profiles as a result of intense erosion episodes stripping pre-existing alteration zones. The periods from Early Barremian to Early Aptian and from Early Barremian to Middle Albian are characterised by significant tectonic inversion events (Crittenden et al., 1998; Indrevær et al., 2017; Oakman & Partington, 1998; Ziegler, 1975). Differential uplift induced by reactivation of inherited basement faults has led to erosion of existing weathering surfaces and exposure of less weathered basement rocks in regions such as the southwestern Norwegian shelf of the Barents Sea (Johannessen et al., 2013; Ksienzyk et al., 2014; Redfield et al., 2005). Tectonic inversion events, such as those documented in the Loppa High, can reshape the local topography, promoting differential erosion and revealing diverse source rocks (Indrevær et al., 2017). In the northern North Sea, tectonic inversion events probably led to the exposure of different source rocks with heterogeneous preservation of saprolite over short distances (Lidmar-Bergström et al., 2009; Migoń & Lidmar-Bergström, 2001). These geological variations played a pivotal role in the formation of chlorite through its precursor minerals within weathered sediments.

5.3 | What are the implications of chlorite development in deep marine siliciclastic reservoirs?

The development of chlorite in the Agat Formation is governed by an intricate interplay of factors related to sediment source composition, the intensity of chemical weathering, and basin configuration/depositional environment. These diverse controls collectively influence the availability of detrital clay precursors, early diagenetic pore water chemistry, burial temperature evolution, and the distribution patterns of chlorite within reservoir units. These complex interactions and their effects on chlorite development are outlined in the subsequent sections and summarised in Figure 17.

5.3.1 | Controls on the source materials (precursors) of chlorite

The composition of the source and the intensity of chemical weathering will have a direct control on the detrital composition of the sediments, which in return will influence the composition and chemistry of chlorite.

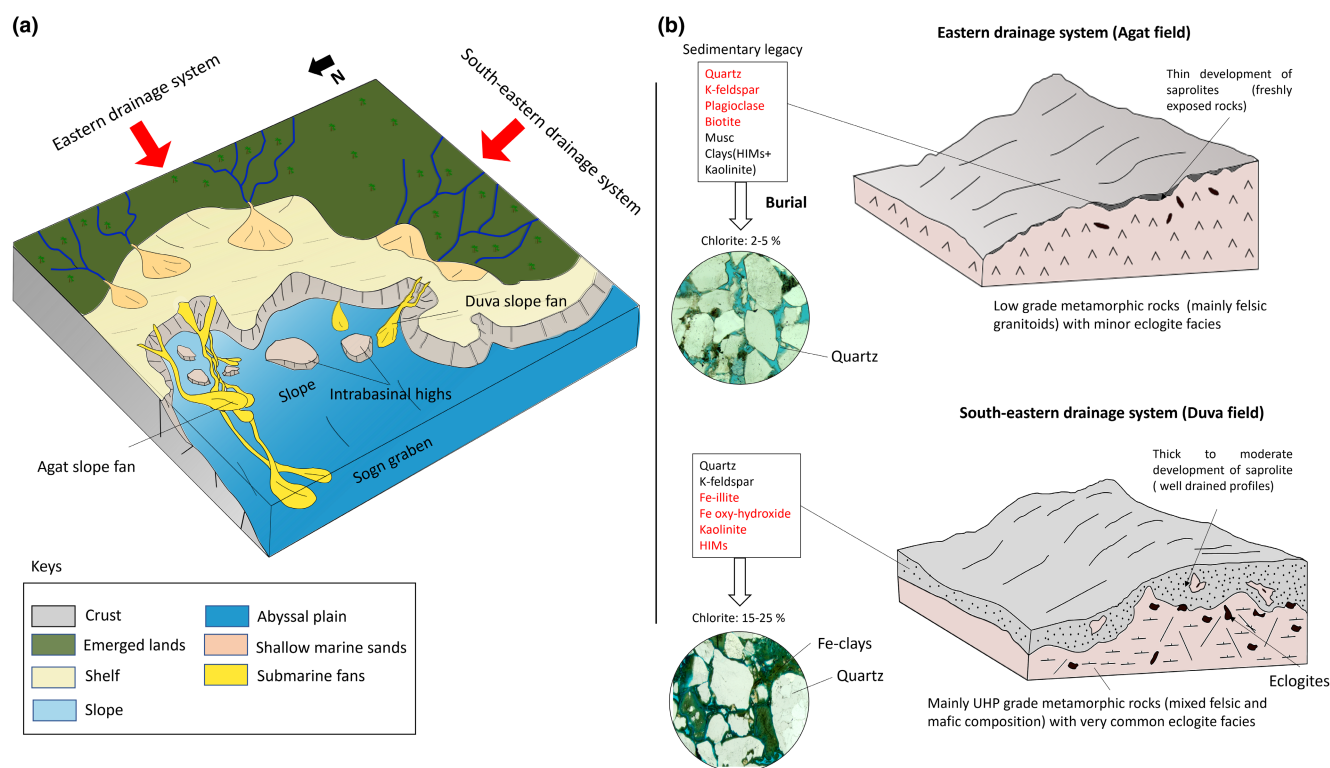


FIGURE 17 (a) Paleogeographic reconstruction of the Agat Fm depositional environment during the Albian-Aptian period (adapted from Gradstein et al., 2016). The deposition in the Agat field occurs in a relatively open area in contrast to the confined character of the duva field. Note that the morphology of turbidite systems was controlled by the complex inherited topography and the presence of intrabasinal relief and highs; (b) Schematic representation of the drainage system in the South and the East showing a significant change in the source composition and the degree of chemical alteration which influence directly the sedimentary legacy and chlorite content.

The sandstone in the Duva field is sourced from a variety of rocks, having a mixed mafic and felsic composition (with some ultramafic rocks), including eclogites, quartzo-feldspathic gneisses, and granitoids, which have undergone extensive chemical alteration. The development of thick alteration profiles (saprolites or laterites) over this mixed rock composition has produced large amounts of fine fraction materials which was likely rich in kaolinite, vermiculite, Fe-rich oxy-hydroxides, and hydroxy-interlayered clays (HIMs) such hydroxy-interlayered smectite (HIS) and hydroxy-interlayered vermiculite (HIV) (Patrier et al., 2023) (Figure 17b). These materials were transported into shallow marine settings allowing the formation of large amount of glauconitic materials and Fe-illite through interaction with seawater (Azzam et al., 2022). Some phosphatic concretions were also formed at this time. These highly Fe-rich materials were remobilised into deep marine settings forming precursors for the development of authigenic Fe-clays during diagenesis, such as berthierine and then chlorite.

The chemistry of chlorite in the Duva field is extremely rich in iron ($X_{Fe} > 0.88$), reflecting the wide availability of ferrous iron in the sandstone during diagenesis. As a result, nearly all the Fe-Al-rich detrital materials were transformed into chlorite. However, in the LR, the fine fraction materials and Fe content were extremely high, leading to excessive development of chlorite and the formation of thick coats around detrital grains reaching up to 30 μm in size (Azzam et al., 2022). The presence of these coats has negatively impacted the reservoir quality by reducing the permeability through decreasing connectivity of the pore network. Conversely, in the UR, the sandstone is clean, containing smaller amounts of fine materials with moderate Fe content, which favours the development of thin chlorite coats. These coats play a positive role by inhibiting quartz overgrowth while preserving the primary intergranular porosity. This suggests that Fe-rich sands, such as the LR, are risky targets for reservoir exploration, despite the wide occurrence of chlorite. Conversely, weaker input of fine fraction materials from saprolites is more suitable for the development of thin chlorite coats.

The sediment source for the Agat field primarily comprises felsic rocks, such as granitic gneisses, which have undergone minimal chemical weathering or had their alteration profiles eroded at an early stage. The raw materials provided from the erosion of these rocks are highly rich in quartz, feldspar (both Na and K-feldspar), biotite, muscovite, and variable amounts of clays (mainly HIMs and kaolinite). The bulk chemistry of this mineralogical assembly is rich in SiO_2 and Al_2O_3 but low in Fe_2O_3 . Chlorite development under low Fe conditions depends on many factors, such as the type of clay precursors, the

availability of ferrous iron, and the redox conditions. In the Agat field, chlorite mainly forms by replacing early detrital clays like HIMs and kaolinite through an intermediate berthierine precursor (Azzam et al., 2023). The source of Fe is typically related to biotite grains containing a considerable amount of Mg and to Ferric clays. The Fe content provided by the dissolution of these grains was low to moderate but was sufficient to transform most of the clay precursors into Fe-chlorite while leaving some residual clay precursor (Figure 5h). The chemistry of these chlorites is highly magnesian (X_{Fe} ca. 0.7) reflecting moderate availability of ferrous iron during sandstone diagenesis.

In summary, chlorite does not necessarily require a strong input of Fe-rich materials to form. A weak to moderate input of Fe-rich materials from saprolites or laterites is more suitable for the development of thin chlorite coats that preserve primary intergranular porosity.

5.3.2 | Controls on chlorite distribution

The distribution of chlorite in the Agat Fm cannot only be explained by provenance and supergene alteration. While chlorite mainly occurs in the form of coatings in the Duva field, it shows a more complex distribution in the Agat field, with a variable amount of pore-filling and pore-lining chlorites. This difference can be related to changes in the depositional processes and transport conditions in deep marine settings. In the case of the Duva field, the sediments are transported within confined incised channels. The sandstones are massive and homogenous showing no evidence of dewatering structures. According to Azzam et al. (2022), chlorite in the Duva field replaces early detrital coats that were formed in shallow marine environments. The confined character of the turbidite system and the narrow shelf probably allowed the preservation of these coats during transportation (Azzam et al., 2022). In the Agat field, the depositional environment is more complex, characterised by a longer transportation distance and deposition in open and less confined settings. Rapid sedimentation in the Agat field often leads to the formation of dish-and-pipe dewatering structures, particularly within lobe and channel deposits. The intensity of dewatering processes plays a crucial role in determining the distribution and concentration of chlorite within the Agat field (Azzam et al., 2023). Pore-filling chlorites dominate in Agat 50 and Agat 100, composed of distal lobe deposits and mud-rich channel deposits, respectively, while chlorite coats dominate in Agat 70 and Agat 80, composed of lobe deposits and weakly confined channel complexes, respectively (Azzam et al., 2023).

5.4 | Improving chlorite predictive models: Moving towards a universal model for Fe-chlorite formation?

The Agat Fm highlights the importance of having a holistic understanding of the sediment routing system to improve predictions of chlorite occurrence and distribution in sedimentary basins. Most of the studies focusing on chlorite have been, to some extent, limited to its origin in the sandstone, with poor understanding of the processes occurring in the source area. Dowey et al. (2012) analysed numerous chlorite-coated sandstones worldwide and proposed that the formation of Fe-rich chlorite is favoured near the equator due to enhanced drainage and warmer temperatures. This promotes chemical weathering, which supplies iron oxyhydroxides and detrital aluminium-rich clays across tropical and temperate regions. Ehrenberg (1993) suggested a genetic link between chlorite-coated sandstones, verdine facies, and oolitic ironstone facies, despite their formation in distinct environments. Chamosite-type ironstones represent low-energy equivalents of chlorite-rich sandstones, typically accumulating in shallow marine settings with minimal sedimentation rate and low-energy conditions (Ehrenberg, 1993). Most of the chamosite *ironstone* deposits have been documented during the Cambrian to Devonian periods, mainly forming along the margins of cratonic blocks. A subsequent episode of ironstone formation began during the Late Triassic following the assembly of the supercontinent Pangaea. This continued throughout the Jurassic, persisting into the Cretaceous and Middle Cenozoic eras marked by widespread ironstone deposition (Van Houten & Purucker, 1984). Iron-rich ooids have been discovered in the upper part of the Wealden Group sandstones in the fluvio-deltaic facies association of the Paris Basin, as well as in the Weald Basin (Taylor, 1990; Virolle et al., 2022). Numerous studies have attributed the origin of oolitic ironstones in Western Europe to the development of thick lateritic weathering soils during the early Cretaceous, following successive tectonic events and several sea level falls that resulted in the emersion and erosion of local domains (Barbarand et al., 2018; Meyer, 1976; Taylor, 1990; Thiry et al., 2006). In the Wealden sandstones, the presence of quartz or ironstone nuclei suggests that the detrital grains (iron fragments and quartz) were most likely derived from the lateritic and ferricrete palaeosols located in the eastern Paris Basin (Taylor, 1996). Weathering and erosion processes acting on iron-rich palaeosols bordering the Paris Basin (e.g. Ardennes, Brabant Massifs) facilitated the transport of significant amounts of Fe and Al, primarily in the form of clays (e.g. Kaolinite, HIMs, Vermiculite) and Fe-ooids composed of iron oxyhydroxide (Corentin et al., 2020; Virolle et al., 2022). The incorporation of these

Al- and Fe-bearing minerals into the sediments is believed to be critical for the formation of berthierine within the Paris and Wealden basins (Virolle et al., 2022).

The Agat Fm shares similar mineralogy and diagenetic evolution with the Wealden sandstones. However, the Agat Fm underwent deeper burial. This difference in burial conditions likely explains the prevalence of berthierine in the Wealden sandstones, whereas chlorite dominates the Agat Fm. The Lower Cretaceous sandstone of the Paris Basin serves as a potential candidate for the environmental conditions prevailing during the deposition of the Agat Formation. Fe- and kaolinite-rich soils were widespread across Europe during the Lower Cretaceous period (Migoń & Lidmar-Bergström, 2001). Kaolinitic saprolites with characteristics resembling tropical palaeosols and bauxite have been found in both the southeastern and northwestern regions of southern Norway. Research suggests that the formation of blockfields in southern Norway is partially attributed to chemical weathering (Follestad, 1974; Strømsøe & Paasche, 2011). The exact age of these saprolites remains unclear; however, clay mineral assemblages suggest lateritic-bauxitic weathering processes occurring in a tropical setting predating the Late Cenozoic period (Lidmar-Bergström et al., 1999; Roaldset et al., 1982). Kaolinitic saprolites have been assigned to the Jurassic and Early Cretaceous periods as they occur within landscapes that are likely to have formed in a sub-Mesozoic relief (Lidmar-Bergström et al., 1999). These kaolinitic palaeosols likely served as the primary source of kaolinite and iron-rich materials (hydro-interlayered clays, iron oxyhydroxides) essential for the formation of berthierine/chlorite within the Agat Formation and potentially other geological formations in Norway. This may suggest that chlorite formation was not an isolated event but rather a large-scale, global process influenced by a combination of geological, climatic and tectonic events across Europe. The results of this study hold the potential to improve our ability to predict chlorite occurrence within sedimentary basins, representing a significant advancement in this field.

6 | CONCLUSION

The Agat Fm was deposited during the Lower Cretaceous from a series of turbidite systems displaying strong textural and mineralogical heterogeneity. Two turbidite systems were investigated in this study: the Duva field and the Agat field. The reservoir quality of these deep marine deposits was controlled by the presence of chlorite and by its distribution in the sandstone. Our results allowed the reconstruction of the sediment provenance as well as giving insight into the climate conditions during the Lower Cretaceous.

In the Duva field, the sandstone is supplied from the Western Gneiss Region, from mixed metamorphic rocks, which includes UHP metamorphic rocks like eclogites and probably coesite-bearing rocks, as suggested by the presence of diamonds. These complex bedrocks were subjected to intensive chemical alteration under humid climates allowing the development of thick alteration profiles. In the Agat field, the sandstone is supplied from Western Norway and possibly some parts of Northern Norway. The bedrock is mainly composed of low-grade metamorphic rocks (dominated by granitic composition) with only weak development of alteration profiles. This study highlights the role of supergene alteration of the continental source rocks on the amounts and the distribution of chlorite in the turbidites of the Duva and Agat fields. The erosion of thick alteration profiles can provide abundant Al and Fe-rich fine-grained materials (clay minerals and oxo-hydroxides) into the basin. Such a material allowed subsequently the growth of thick Fe-chlorite coats, which have a negative impact on the reservoir quality. When the sediment is supplied from weakly to non-weathered basement rocks, only thin diagenetic chlorite coats occur, allowing the preservation of good reservoir quality.

The distribution of chlorite, whether in the form of coating or pore-filling, was controlled by the depositional environment and basin configuration, which was related to the inherited topography from Jurassic rifting. Chlorite distribution in fine-grained turbidite systems like the Agat field is likely to be controlled by dewatering processes. Conversely, chlorite in confined coarse-grained turbidite systems could be inherited from shallow marine environments. The mineralogical and textural heterogeneity observed in the Agat Fm suggests a complex interplay between the source, chemical alteration and depositional environment in controlling the distribution and development of chlorite in deep marine deposits. These findings have important implications for predicting chlorite distribution in sedimentary records and can help guide future exploration and development of deep marine deposits.

ACKNOWLEDGEMENTS

This study was funded by Neptune Energy. The authors would like to express their gratitude to Neptune Energy Norge AS, PGNiG Upstream Norway AS, Idemitsu Petroleum Norge AS, Sval Energi AS, and VNG Norge AS for providing access to samples, data and information. Special thanks are extended to Claire Boukari and Frédéric Haurine for their assistance with heavy minerals preparation and U/Pb zircon analysis. We are also grateful to the reviewers (Stuart Jones and an anonymous

reviewer) for their constructive comments and suggestions that improved this paper.

FUNDING INFORMATION

This study was funded by Neptune Energy Norge (Neptune Energy Norge AS 10.13039/100016930).

CONFLICT OF INTEREST STATEMENT

The authors declare that they have no known competing financial interests or personal relationships that could have appeared to influence the work reported in this paper.

DATA AVAILABILITY STATEMENT

Data that support the findings of this study are available on request from the corresponding author.

ORCID

Fares Azzam  <https://orcid.org/0000-0003-2237-3468>

Thomas Blaise  <https://orcid.org/0000-0003-1820-8152>

Ahmed Abd Elmola  <https://orcid.org/0000-0003-3353-0895>

REFERENCES

- Ajdukiewicz, J. M., & Larese, R. E. (2012). How clay grain coats inhibit quartz cement and preserve porosity in deeply buried sandstones: Observations and experiments. *American Association of Petroleum Geologists Bulletin*, 96, 2091–2119. <https://doi.org/10.1306/02211211075>
- Anand, R. R., & Gilkes, R. J. (1984). Weathering of ilmenite in a lateritic pallid zone. *Clays and Clay Minerals*, 32, 363–374. <https://doi.org/10.1346/CCMN.1984.0320504>
- Ansart, C., 2022. *Formation des latérites du bouclier amazonien: Apports du couplage minéralogie—géochimie—géochronologie*. Paris-Saclay University.
- Azzam, F., Blaise, T., Dewla, M., Patrier, P., Beaufort, D., Elmola, A. A., Brigaud, B., Portier, E., Barbarand, J., & Clerc, S. (2023). Role of depositional environment on clay coat distribution in deeply buried turbidite sandstones: Insights from the Agat field, Norwegian North Sea. *Marine and Petroleum Geology*, 155, 106379. <https://doi.org/10.1016/J.MARPETGEO.2023.106379>
- Azzam, F., Blaise, T., Patrier, P., Abd-Elmola, A., Beaufort, D., Portier, E., Brigaud, B., Barbarand, J., & Clerc, S. (2022). Diagenesis and reservoir quality evolution of the Lower Cretaceous turbidite sandstones of the Agat Formation (Norwegian North Sea): Impact of clay grain coating and carbonate cement. *Marine and Petroleum Geology*, 142, 105768. <https://doi.org/10.1016/j.marpetgeo.2022.105768>
- Barbarand, J., Bour, I., Pagel, M., Quesnel, F., Delcambre, B., Dupuis, C., & Yans, J. (2018). Post-Paleozoic evolution of the northern Ardenne Massif constrained by apatite fission-track thermochronology and geological data. *BSGF Earth Sciences Bulletin*, 189, 16. <https://doi.org/10.1051/bsgf/2018015>
- Basu, A., Young, S. W., Suttner, L. J., James, W. C., & Mack, G. H. (1975). Re-evaluation of the use of undulatory extinction and

- polycrystallinity in detrital quartz for provenance interpretation. *Journal of Sedimentary Research*, 45, 873–882. <https://doi.org/10.1306/212F6E6F-2B24-11D7-8648000102C1865D>
- Bauck, M., Faleide, J. I., & Fossen, H. (2021). Late Jurassic to Late Cretaceous canyons on the Måløy Slope: Source to sink fingerprints on the northernmost North Sea rift margin, Norway. *Norwegian Journal of Geology*, 101, 1–30. <https://doi.org/10.17850/njg101-3-1>
- Beaufort, D., Rigault, C., Billon, S., Billault, V., Inoue, A., Inoue, S., & Patrier, P. (2015). Chlorite and chloritization processes through mixed-layer mineral series in low-temperature geological systems—A review. *Clay Minerals*, 50, 497–523. <https://doi.org/10.1180/claymin.2015.050.4.06>
- Billault, V., Beaufort, D., Baronnet, A., & Lacharpagne, J.-C. (2003). A nanopetrographic and textural study of grain-coating chlorites in sandstone reservoirs. *Clay Minerals*, 38, 315–328. <https://doi.org/10.1180/0009855033830098>
- Bingen, B., & Solli, A. (2009). Geochronology of magmatism in the Caledonian and Sveconorwegian belts of Baltica: Synopsis for detrital zircon provenance studies. *Norsk Geologisk Tidsskrift*, 89, 267–290.
- Bloch, S., Lander, R. H., & Bonnell, L. (2002). Anomalously high porosity and permeability in deeply buried sandstone reservoirs: Origin and predictability. *American Association of Petroleum Geologists Bulletin*, 86, 301–328. <https://doi.org/10.1306/61eedabc-173e-11d7-8645000102c1865d>
- Blott, S. J., & Pye, K. (2001). GRADISTAT: A grain size distribution and statistics package for the analysis of unconsolidated sediments. *Earth Surface Processes and Landforms*, 26, 1237–1248. <https://doi.org/10.1002/ESP.261>
- Bouma, A. H. (2000). Coarse-grained and fine-grained turbidite systems as end member models: Applicability and dangers. *Marine and Petroleum Geology*, 17, 137–143. [https://doi.org/10.1016/S0264-8172\(99\)00020-3](https://doi.org/10.1016/S0264-8172(99)00020-3)
- Bouma, A. H. (2004). Key controls on the characteristics of turbidite systems. *Geological Society—Special Publications*, 222, 9–22. <https://doi.org/10.1144/GSL.SP.2004.222.01.02>
- Braun, J. J., Pagel, M., Muller, J. P., Bilong, P., Michard, A., & Guillet, B. (1990). Cerium anomalies in lateritic profiles. *Geochimica et Cosmochimica Acta*, 54, 781–795. [https://doi.org/10.1016/0016-7037\(90\)90373-S](https://doi.org/10.1016/0016-7037(90)90373-S)
- Brekke, H. (2000). The tectonic evolution of the Norwegian Sea continental margin with emphasis on the Voring and More Basins. *Geological Society Special Publication*, 167, 327–378. <https://doi.org/10.1144/GSL.SP.2000.167.01.13>
- Bugge, T., Tveiten, B., & Bäckström, S. (2001). The depositional history of the cretaceous in the northeastern North Sea. *Norwegian Petroleum Society Special Publications*, 10, 279–291. [https://doi.org/10.1016/S0928-8937\(01\)80018-7](https://doi.org/10.1016/S0928-8937(01)80018-7)
- Bukta, K. E. (2018). *Slørebotn sub-basin tectono-stratigraphic framework*. The University of Stavanger.
- Butler, J. P., Jamieson, R. A., Steenkamp, H. M., & Robinson, P. (2013). Discovery of coesite–eclogite from the Nordøyane UHP domain, Western Gneiss Region, Norway: Field relations, metamorphic history, and tectonic significance. *Journal of Metamorphic Geology*, 31, 147–163. <https://doi.org/10.1111/jmg.12004>
- Chen, M., Sun, M., Cai, K., Buslov, M. M., Zhao, G., & Rubanova, E. S. (2014). Geochemical study of the Cambrian–Ordovician meta-sedimentary rocks from the northern Altai–Mongolian terrane, northwestern Central Asian Orogenic Belt: Implications on the provenance and tectonic setting. *Journal of Asian Earth Sciences*, 96, 69–83. <https://doi.org/10.1016/j.jseas.2014.08.028>
- Clark, S. P. (1966). Section 1: Composition of rocks. In *Handbook of physical constants* (pp. 1–6). Geological Society of America. <https://doi.org/10.1130/MEM97-p1>
- Corentin, P., Deconinck, J.-F., Pellenard, P., Amédéo, F., Bruneau, L., Chenot, E., Matrimon, B., Huret, E., & Landrein, P. (2020). Environmental and climatic controls of the clay mineralogy of Albian deposits in the Paris and Vocontian basins (France). *Cretaceous Research*, 108, 104342. <https://doi.org/10.1016/j.cretres.2019.104342>
- Cornu, S., Lucas, Y., Lebon, E., Ambrosi, J. P., Luizão, F., Rouiller, J., Bonnay, M., & Neal, C. (1999). Evidence of titanium mobility in soil profiles, Manaus, central Amazonia. *Geoderma*, 91, 281–295. [https://doi.org/10.1016/S0016-7061\(99\)00007-5](https://doi.org/10.1016/S0016-7061(99)00007-5)
- Craigie, N. (2018). Geochemistry and mineralogy. In *Principles of elemental chemostratigraphy: A practical user guide* (pp. 39–83). Springer International Publishing. https://doi.org/10.1007/978-3-319-71216-1_3
- Crittenden, S., Cole, J. M., & Kirk, M. J. (1998). The distribution of Aptian sandstones in the central and northern North Sea (UK sector)—A lowstand systems tract play. Part 2: Distribution and exploration strategy. *Journal of Petroleum Geology*, 21, 187–211. <https://doi.org/10.1111/j.1747-5457.1998.tb00653.x>
- Cuthbert, S. J., Carswell, D. A., Krogh-Ravna, E. J., & Wain, A. (2000). Eclogites and eclogites in the Western Gneiss Region, Norwegian Caledonides. *Lithos*, 52, 165–195. [https://doi.org/10.1016/S0024-4937\(99\)00090-0](https://doi.org/10.1016/S0024-4937(99)00090-0)
- Deepthy, R., & Balakrishnan, S. (2005). Climatic control on clay mineral formation: Evidence from weathering profiles developed on either side of the Western Ghats. *Journal of Earth System Science*, 114, 545–556. <https://doi.org/10.1007/BF02702030>
- Dowey, P. J., Hodson, D. M., & Worden, R. H. (2012). Pre-requisites, processes, and prediction of chlorite grain coatings in petroleum reservoirs: A review of subsurface examples. *Marine and Petroleum Geology*, 32, 63–75. <https://doi.org/10.1016/j.marpetgeo.2011.11.007>
- Duteil, T., Bourillot, R., Grégoire, B., Virolle, M., Brigaud, B., Nouet, J., Braissant, O., Portier, E., Féliès, H., Patrier, P., Gontier, E., Svahn, I., & Visscher, P. T. (2020). Experimental formation of clay-coated sand grains using diatom biofilm exopolymers. *Geology*, 48, 1012–1017. <https://doi.org/10.1130/G47418.1/5074182/g47418.pdf>
- Ehrenberg, S. N. (1993). Preservation of anomalously high porosity in deeply buried sandstones by grain-coating chlorite: Examples from the Norwegian continental shelf. *American Association of Petroleum Geologists Bulletin*, 77, 1260–1286. <https://doi.org/10.1306/f4c8e062-1712-11d7-8645000102c1865d>
- Follestad, B. A. (1974). Tangen. Beskrivelse til kvartaergeologisk kart 1916 II—M 1:50 000 med fargetrykt kart. *Norges Geologiske Undersøkelse*, 313, 62.
- Fossen, H., Cavalcante, G. C., & de Almeida, R. P. (2017). Hot versus cold orogenic behavior: Comparing the Araçuaí–West Congo and the Caledonian Orogens. *Tectonics*, 36, 2159–2178. <https://doi.org/10.1002/2017TC004743>
- Fredin, O., Viola, G., Zwingmann, H., Sørli, R., Brønner, M., Lie, J. E., Grandal, E. M., Müller, A., Margreth, A., Vogt, C., & Knies, J. (2017). The inheritance of a mesozoic landscape in western Scandinavia. *Nature Communications*, 8. <https://doi.org/10.1038/ncomms14879>

- Gärtner, A., Linnemann, U., Sagawe, A., Hofmann, M., Ullrich, B., & Kleber, A. (2013). Morphology of zircon crystal grains in sediments—Characteristics, classifications, definitions Morphologie von zirkonen in sedimenten—Merkmale, klassifikationen, definitionen. *Journal of Central European Geology*, 59, 65–73.
- Giles, M. R., Stevenson, S., Martin, S. V., Cannon, S. J. C., Hamilton, P. J., Marshall, J. D., & Samways, G. M. (1992). The reservoir properties and diagenesis of the Brent Group: A regional perspective. *Geological Society, London, Special Publications*, 61, 289–327. <https://doi.org/10.1144/GSL.SP.1992.061.01.16>
- Glennie, K. W. (2009). Petroleum geology of the North Sea: Basic concepts and recent advances: Fourth edition. In *Petroleum Geology of the North Sea: Basic Concepts and Recent Advances: Fourth Edition* (pp. 245–293). Wiley. <https://doi.org/10.1002/9781444313413>
- Goldberg, K., & Humayun, M. (2010). The applicability of the Chemical Index of Alteration as a paleoclimatic indicator: An example from the Permian of the Paraná Basin, Brazil. *Palaeogeography Palaeoclimatology Palaeoecology*, 293, 175–183. <https://doi.org/10.1016/j.palaeo.2010.05.015>
- Gradstein, F. M., Waters, C. N., Charnock, M., Munsterman, D., Hollerbach, M., Brunstad, H., Hammer, Ø., & Vergara, L. (2016). Stratigraphic guide to the Cromer Knoll, Shetland and Chalk groups, North Sea and Norwegian Sea. *Newsletters on Stratigraphy*, 49, 73–280. <https://doi.org/10.1127/nos/2016/0071>
- Griffiths, J., Worden, R. H., Utley, J. E. P., Broström, C., Martinius, A. W., Lawan, A. Y., & Al-Hajri, A. I. (2021). Origin and distribution of grain-coating and pore-filling chlorite in deltaic sandstones for reservoir quality assessment. *Marine and Petroleum Geology*, 134, 105326. <https://doi.org/10.1016/j.marpetgeo.2021.105326>
- Hansen, H. N., Løvstad, K., Lageat, G., Clerc, S., & Jahren, J. (2021). Chlorite coating patterns and reservoir quality in deep marine depositional systems—Example from the Cretaceous Agat Formation, Northern North Sea, Norway. *Basin Research*, 33, 2725–2744. <https://doi.org/10.1111/BRE.12581>
- Heinrich, B., & Nicole, D. (2011). Chapter 6. A review of the Chemical Index of Alteration (CIA) and its application to the study of Neoproterozoic glacial deposits and climate transitions. *Geological Society, London, Memoirs*, 36, 81–92. <https://doi.org/10.1144/M36.6>
- Heiri, O., Lotter, A. F., & Lemcke, G. (2001). Loss on ignition as a method for estimating organic and carbonate content in sediments: Reproducibility and comparability of results. *Journal of Paleolimnology*, 25, 101–110. <https://doi.org/10.1023/A:1008119611481>
- Hugo, V., & Cornell, D. H. (1991). Altered ilmenites in Holocene dunes from Zululand, South Africa: Petrographic evidence for multistage alteration. *South African Journal of Geology*, 94, 365–378.
- Indrevær, K., Gabrielsen, R. H., & Faleide, J. I. (2017). Early Cretaceous synrift uplift and tectonic inversion in the Loppa high area, southwestern Barents Sea, Norwegian shelf. *Journal of the Geological Society*, 174, 242–254. <https://doi.org/10.1144/jgs2016-066>
- Jackson, C. A. L., Barber, G. P., & Martinsen, O. J. (2008). Submarine slope morphology as a control on the development of sand-rich turbidite depositional systems: 3D seismic analysis of the Kyrre Fm (Upper Cretaceous), Måløy Slope, offshore Norway. *Marine and Petroleum Geology*, 25, 663–680. <https://doi.org/10.1016/j.marpetgeo.2007.12.007>
- Johannessen, K., Kohlmann, F., Ksienzyk, A., Dunkl, I., & Jacobs, J. (2013). Tectonic evolution of the SW Norwegian passive margin based on low-temperature thermochronology from the innermost Hardangerfjord. *Norsk Geologisk Tidsskrift*, 93, 242–260.
- Knudsen, C., Thomsen, T. B., Kalsbeek, F., Kristensen, J. A., Vital, H., & McLimans, R. K. (2015). Composition of ilmenite and provenance of zircon in northern Brazil. *Geological Survey of Denmark and Greenland Bulletin*, 33, 81–84. <https://doi.org/10.34194/geusb.v33.4515>
- Kotowski, J., Nejbert, K., & Olszewska-Nejbert, D. (2020). Tourmalines as a tool in provenance studies of Terrigenous material in extra-Carpathian Albian (Uppermost Lower Cretaceous) sands of Miechów Synclinorium, Southern Poland. *Minerals*, 10, 0917. <https://doi.org/10.3390/min10100917>
- Krumbein, W. C. (1963). *Stratigraphy and sedimentation* (2nd ed.). W.H. Freeman.
- Ksienzyk, A., Dunkl, I., Jacobs, J., Fossen, H., & Kohlmann, F. (2014). From orogen to passive margin: Constraints from fission track and (U-Th)/He analyses on Mesozoic uplift and fault reactivation in SW Norway. *Geological Society of London, Special Publication*, 390, 679–702. <https://doi.org/10.1144/SP390.27>
- Lidmar-Bergström, K., Olsson, S., & Olvmo, M. (1997). *Palaeosurfaces and associated saprolites in southern Sweden* (pp. 95–124). Geological Society London Special Publications.
- Lidmar-Bergström, K., Olsson, S., & Roaldset, E. (1999). *Relief features and palaeoweathering remnants in formerly glaciated Scandinavian basement areas* (pp. 275–301). Special Publication of the International Association of Sedimentologists.
- Lidmar-Bergström, K., Olsson, S., & Roaldset, E. (2009). Relief features and palaeoweathering remnants in formerly glaciated Scandinavian basement areas. In *Palaeoweathering, palaeosurfaces and related continental deposits* (Vol. 27, pp. 275–301). International Association of Sedimentologists Special Publications. <https://doi.org/10.1002/9781444304190.ch11>
- Lien, T., Midtbø, R. E., & Martinsen, O. J. (2006). Depositional facies and reservoir quality of deep-marine sandstones in the Norwegian Sea. *Norsk Geologisk Tidsskrift*, 86, 71–92.
- Loveland, P. J. (1984). The soil clays of Great Britain: I. England and Wales. *Clay Minerals*, 19, 681–707. <https://doi.org/10.1180/claymin.1984.019.5.02>
- Ludwig, K. R. (1998). On the treatment of concordant uranium-lead ages. *Geochimica et Cosmochimica Acta*, 62(4), 665–676. [https://doi.org/10.1016/S0016-7037\(98\)00059-3](https://doi.org/10.1016/S0016-7037(98)00059-3)
- Martinsen, O. J., Lien, T., & Jackson, C. (2005). Cretaceous and Palaeogene turbidite systems in the North Sea and Norwegian Sea basins: Source, staging area and basin physiography controls on reservoir development. *Petroleum Geology Conference Proceedings*, 6, 1147–1164. <https://doi.org/10.1144/0061147>
- McLennan, S. M. (1989). Rare earth elements in sedimentary rocks; influence of provenance and sedimentary processes. *Reviews in Mineralogy and Geochemistry*, 21, 169–200.
- Meunier, A., Caner, L., Hubert, F., El Albani, A., & Pret, D. (2013). The weathering intensity scale (WIS): An alternative approach of the chemical index of alteration (CIA). *American Journal of Science*, 313, 113–143. <https://doi.org/10.2475/02.2013.03>
- Meyer, R. (1976). Continental sedimentation, soil genesis and marine transgression in the basal beds of the Cretaceous in the

- east of the Paris Basin. *Sedimentology*, 23, 235–253. <https://doi.org/10.1111/j.1365-3091.1976.tb00048.x>
- Migoń, P., & Lidmar-Bergström, K. (2001). Weathering mantles and their significance for geomorphological evolution of central and northern Europe since the Mesozoic. *Earth-Science Reviews*, 56, 285–324. [https://doi.org/10.1016/S0012-8252\(01\)00068-X](https://doi.org/10.1016/S0012-8252(01)00068-X)
- Morad, S., Ketzer, J. M., & De Ros, L. F. (2013). Linking diagenesis to sequence stratigraphy: An integrated tool for understanding and predicting reservoir quality distribution. In *Linking diagenesis to sequence stratigraphy* (Vol. 45, pp. 1–36). International Association of Sedimentologists Special Publications. <https://doi.org/10.1002/9781118485347.ch1>
- Morton, A., Hallsworth, C., & Chalton, B. (2004). Garnet compositions in Scottish and Norwegian basement terrains: A framework for interpretation of North Sea sandstone provenance. *Marine and Petroleum Geology*, 21, 393–410. <https://doi.org/10.1016/j.marpetgeo.2004.01.001>
- Morton, A. C., & Hallsworth, C. (1994). Identifying provenance-specific features of detrital heavy mineral assemblages in sandstones. *Sedimentary Geology*, 90, 241–256. [https://doi.org/10.1016/0037-0738\(94\)90041-8](https://doi.org/10.1016/0037-0738(94)90041-8)
- Morton, A. C., & Hallsworth, C. R. (1999). Processes controlling the composition of heavy mineral assemblages in sandstones. *Sedimentary Geology*, 124, 3–29. [https://doi.org/10.1016/S0037-0738\(98\)00118-3](https://doi.org/10.1016/S0037-0738(98)00118-3)
- Mücke, A., & Bhadra Chaudhuri, J. N. (1991). The continuous alteration of ilmenite through pseudorutile to leucoxene. *Ore Geology Reviews*, 6, 25–44. [https://doi.org/10.1016/0169-1368\(91\)90030-B](https://doi.org/10.1016/0169-1368(91)90030-B)
- Murakami, T., Ito, J.-I., Utsunomiya, S., Kasama, T., Kozai, N., & Ohnuki, T. (2004). Anoxic dissolution processes of biotite: Implications for Fe behavior during Archean weathering. *Earth and Planetary Science Letters*, 224, 117–129. <https://doi.org/10.1016/j.epsl.2004.04.040>
- Oakman, C. D., & Partington, M. A. (1998). Petroleum geology of the North Sea. In K. W. Glennie (Ed.), *Cretaceous petroleum geology of the North Sea, basic concepts and recent advances* (Vol. 294–349, 4th ed., pp. 294–349). Blackwell Scientific. [https://doi.org/10.1016/s0037-0738\(00\)00100-7](https://doi.org/10.1016/s0037-0738(00)00100-7)
- Odin, G. S. (1988). *Green marine clays: Oolitic ironstone facies, verdine facies, glaucony facies and celadonite-bearing facies—A comparative study*. *Green marine clays: Oolitic ironstone facies, verdine facies, glaucony facies and celadonite-bearing facies—A comparative study* (Vol. 27, pp. 396–397). Elsevier. [https://doi.org/10.1016/0012-8252\(90\)90077-9](https://doi.org/10.1016/0012-8252(90)90077-9)
- Olesen, O., Bering, D., Brønner, M., Dalsegg, E., Fabian, K., Fredin, O., Gellein, J., Husteli, B., Magnus, C., Rønning, J. S., & Solbakk, T. (2012). NGU Report 2012.005 Tropical Weathering in Norway, TWIN Final Report 188.
- Patrier, P., Beaufort, D., Azzam, F., Blaise, T., Portier, E., Brigaud, B., & Clerc, S. (2023). New insights on diagenetic chlorite and its source material in turbiditic sandstones of contrasted reservoir quality in the lower cretaceous Agat formation (Duva oil and gas field, northern Norwegian North Sea). *Marine and Petroleum Geology*, 152, 106221. <https://doi.org/10.1016/j.marpetgeo.2023.106221>
- Porten, K. W., Warchoń, M. J., & Kane, I. A. (2019). Formation of detrital clay grain coats by dewatering of deep-water sands and significance for reservoir quality. *Journal of Sedimentary Research*, 89, 1231–1249. <https://doi.org/10.2110/jsr.2019.65>
- Price, J. R., & Velbel, M. A. (2014). Rates of biotite weathering, and clay mineral transformation and Neof ormation, determined from watershed geochemical mass-balance methods for the Coweeta hydrologic laboratory, southern blue Ridge Mountains, North Carolina, USA. *Aquatic Geochemistry*, 20, 203–224. <https://doi.org/10.1007/s10498-013-9190-y>
- Ravna, E. J. K., Kullerud, K., & Ellingsen, E. (2006). Prograde garnet-bearing ultramafic rocks from the Tromsø Nappe, northern Scandinavian Caledonides. *Lithos*, 92, 336–356. <https://doi.org/10.1016/j.lithos.2006.03.058>
- Redfield, T. F., Osmundsen, P. T., & Hendriks, B. W. H. (2005). The role of fault reactivation and growth in the uplift of western Fennoscandia. *Journal of the Geological Society*, 162, 1013–1030. <https://doi.org/10.1144/0016-764904-149>
- Roaldset, E., Pettersen, E., Longva, O., & Mangerud, J. (1982). Remnants of preglacial weathering in western Norway. *Norsk Geologisk Tidsskrift*, 62, 169–178.
- Roduit, N. (2007). Un logiciel d'analyse d'images pétrographiques polyvalent.
- Rudnick, R., & Gao, S. (2003). Composition of the continental crust. *Treatise on Geochemistry*, 3, 1–64. <https://doi.org/10.1016/B0-08-043751-6/03016-4>
- Ryan, P. C., & Hillier, S. (2002). Berthierine/chamosite, corrensite, and discrete chlorite from evolved verdine and evaporite-associated facies in the Jurassic Sundance formation, Wyoming. *American Mineralogist*, 87, 1607–1615. <https://doi.org/10.2138/am-2002-11-1210>
- Saiğ, J., Brigaud, B., Portier, É., Desaubliaux, G., Bucherie, A., Miska, S., & Pagel, M. (2016). Sedimentological control on the diagenesis and reservoir quality of tidal sandstones of the upper Cape Hay formation (Permian, Bonaparte Basin, Australia). *Marine and Petroleum Geology*, 77, 597–624. <https://doi.org/10.1016/j.marpetgeo.2016.07.002>
- Schmidt, V., & McDonald, D. A. (1979). Texture and recognition of secondary porosity in sandstones. In P. A. Scholle & P. R. Schluger (Eds.), *Aspects of diagenesis: Society of economic paleontologists and mineralogists special publication* (Vol. 26, pp. 209–225). Society of Economic Paleontologists and Mineralogists. <https://doi.org/10.2110/PEC.79.26.0209>
- Sharma, A., & Rajamani, V. (2000). Weathering of gneissic rocks in the upper reaches of Cauvery river, south India: Implications to neotectonics of the region. *Chemical Geology*, 166, 203–223. [https://doi.org/10.1016/S0009-2541\(99\)00222-3](https://doi.org/10.1016/S0009-2541(99)00222-3)
- Singer, A. (1984). The paleoclimatic interpretation of clay minerals in sediments—A review. *Earth Science Reviews*, 21, 251–293. [https://doi.org/10.1016/0012-8252\(84\)90055-2](https://doi.org/10.1016/0012-8252(84)90055-2)
- Skibeli, M., Barnes, K., Straume, T., Syvertsen, S. E., & Shanmugam, G. (1995). A sequence stratigraphic study of Lower Cretaceous deposits in the northernmost North Sea. *Norwegian Petroleum Society Special Publications*, 5, 389–400. [https://doi.org/10.1016/S0928-8937\(06\)80077-9](https://doi.org/10.1016/S0928-8937(06)80077-9)
- Strømsoe, J. R., & Paasche, Ø. (2011). Weathering patterns in high-latitude regolith. *Journal of Geophysical Research: Earth Surface*, 116, 12–15. <https://doi.org/10.1029/2010JF001954>
- Sugimori, H., Yokoyama, T., & Murakami, T. (2009). Kinetics of biotite dissolution and Fe behavior under low O₂ conditions and their implications for Precambrian weathering. *Geochimica et Cosmochimica Acta*, 73, 3767–3781. <https://doi.org/10.1016/j.gca.2009.03.034>
- Surdam, R. C., Crossey, L. J., Hagen, E. S., & Heasler, H. P. (1989). Organic-inorganic interactions and sandstone diagenesis.

- American Association of Petroleum Geologists Bulletin*, 73, 1–23. <https://doi.org/10.1306/703c9ad7-1707-11d7-8645000102c1865d>
- Taylor, G., & Eggleton, R. A. (2001). Regolith geology and geomorphology.
- Taylor, K. (1990). Berthierine from the non-marine Wealden (Early Cretaceous) sediments of South-East England. *Clay Minerals*, 25, 391–399. <https://doi.org/10.1180/claymin.1990.025.3.13>
- Taylor, K. G. (1996). Early cretaceous iron ooids in the Paris Basin: Pedogenic versus marine origin and their palaeoclimatic significance. *Cretaceous Research*, 17, 109–118. <https://doi.org/10.1006/cres.1996.0009>
- Taylor, S. R., & McLennan, S. M. (1985). *The continental crust: Its composition and evolution*. Blackwell Scientific Publications.
- Thiry, M. (2000). Palaeoclimatic interpretation of clay minerals in marine deposits: An outlook from the continental origin. *Earth Science Reviews*, 49, 201–221. [https://doi.org/10.1016/S0012-8252\(99\)00054-9](https://doi.org/10.1016/S0012-8252(99)00054-9)
- Thiry, M., Quesnel, F., Yans, J., Wyns, R., Vergari, A., Theveniaut, H., Simon-Coinçon, R., Ricordel, C., Moreau, M.-G., Giot, D., Dupuis, C., Bruxelles, L., Barbarand, J., & Baele, J.-M. (2006). Continental France and Belgium during the early cretaceous: Paleoweatherings and paleolandforms. *Bulletin de la Société Géologique de France*, 177, 155–175. <https://doi.org/10.2113/gssgfbull.177.3.155>
- Tijani, M. N., Okunlola, O. A., & Abimbola, A. F. (2006). Lithogenic concentrations of trace metals in soils and saprolites over crystalline basement rocks: A case study from SW Nigeria. *Journal of African Earth Sciences*, 46, 427–438. <https://doi.org/10.1016/j.jafrearsci.2006.08.003>
- Van Houten, F. B., & Purucker, M. E. (1984). Glauconitic peloids and chamositic ooids—Favorable factors, constraints, and problems. *Earth Science Reviews*, 20, 211–243. [https://doi.org/10.1016/0012-8252\(84\)90002-3](https://doi.org/10.1016/0012-8252(84)90002-3)
- Vermeesch, P. (2018). IsoplotR: A free and open toolbox for geochronology. *Geoscience Frontiers*, 9, 1479–1493. <https://doi.org/10.1016/j.gsf.2018.04.001>
- Virolle, M., Brigaud, B., Beaufort, D., Patrier, P., Abdelrahman, E., Thomas, H., Portier, E., Samson, Y., Bourillot, R., & Féliès, H. (2022). Authigenic berthierine and incipient chloritization in shallowly buried sandstone reservoirs: Key role of the source-to-sink context. *GSA Bulletin*, 134, 739–761. <https://doi.org/10.1130/b35865.1>
- Virolle, M., Brigaud, B., Bourillot, R., Féliès, H., Portier, E., Duteil, T., Nouet, J., Patrier, P., & Beaufort, D. (2019). Detrital clay grain coats in estuarine clastic deposits: Origin and spatial distribution within a modern sedimentary system, the Gironde estuary (south-west France). *Sedimentology*, 66, 859–894. <https://doi.org/10.1111/sed.12520>
- Wang, J., Wu, C., Li, Z., Zhu, W., Zhou, T., Wu, J., & Wang, J. (2019). Whole-rock geochemistry and zircon Hf isotope of Late Carboniferous–Triassic sediments in the Bogda region, NW China: Clues for provenance and tectonic setting. *Geological Journal*, 54, 1853–1877. <https://doi.org/10.1002/gj.3110>
- Weibel, R., & Friis, H. (2007). Chapter 10. Alteration of opaque heavy minerals as a reflection of the geochemical conditions in depositional and diagenetic environments. *Developments in Sedimentology*, 58, 277–303. [https://doi.org/10.1016/S0070-4571\(07\)58010-6](https://doi.org/10.1016/S0070-4571(07)58010-6)
- White, A. F., Bullen, T. D., Schulz, M. S., Blum, A. E., Huntington, T. G., & Peters, N. E. (2001). Differential rates of feldspar weathering in granitic regoliths. *Geochimica et Cosmochimica Acta*, 65, 847–869. [https://doi.org/10.1016/S0016-7037\(00\)00577-9](https://doi.org/10.1016/S0016-7037(00)00577-9)
- Wiest, J. D., Jacobs, J., Ksienzyk, A. K., & Fossen, H. (2018). Sveconorwegian vs. Caledonian orogenesis in the eastern Øygarden complex, SW Norway—Geochronology, structural constraints and tectonic implications. *Precambrian Research*, 305, 1–18. <https://doi.org/10.1016/j.precamres.2017.11.020>
- Wooldridge, L. J., Worden, R. H., Griffiths, J., Thompson, A., & Chung, P. (2017). Biofilm origin of clay-coated sand grains. *Geology*, 45, 875–878. <https://doi.org/10.1130/G39161.1>
- Worden, R. H., Griffiths, J., Wooldridge, L. J., Utley, J. E. P., Lawan, A. Y., Muhammed, D. D., Simon, N., & Armitage, P. J. (2020). Chlorite in sandstones. *Earth-Science Reviews*, 204, 103105. <https://doi.org/10.1016/j.earscirev.2020.103105>
- Xiao, M., Yuan, X., Cheng, D., Wu, S., Cao, Z., Tang, Y., & Xie, Z. (2018). Feldspar dissolution and its influence on reservoirs: A case study of the lower Triassic Baikouquan formation in the northwest margin of the Junggar Basin, China. *Geofluids*, 2018, 1–19. <https://doi.org/10.1155/2018/6536419>
- Yuan, G., Cao, Y., Jia, Z., Gluyas, J., Yang, T., Wang, Y., & Xi, K. (2015). Selective dissolution of feldspars in the presence of carbonates: The way to generate secondary pores in buried sandstones by organic CO₂. *Marine and Petroleum Geology*, 60, 105–119. <https://doi.org/10.1016/j.marpetgeo.2014.11.001>
- Ziegler, P. A. (1975). Geologic evolution of North Sea and its tectonic framework. *American Association of Petroleum Geologists Bulletin*, 59, 1073–1097. <https://doi.org/10.1306/83D91F2E-16C7-11D7-8645000102C1865D>
- Ziegler, P. A. (1990). Tectonic and palaeogeographic development of the North Sea rift system. In D. J. Blundell, & A. D. Gibbs (Eds.), *Tectonic evolution of the North Sea rifts* (pp. 1–36). Oxford University Press.

SUPPORTING INFORMATION

Additional supporting information can be found online in the Supporting Information section at the end of this article.

How to cite this article: Azzam, F., Blaise, T., Patrier, P., Beaufort, D., Barbarand, J., Elmola, A. A., Brigaud, B., Portier, E., & Clerc, S. (2024). Impact of sediment provenance and depositional setting on chlorite content in Cretaceous turbiditic sandstones, Norway. *Basin Research*, 36, e12867. <https://doi.org/10.1111/bre.12867>